Characterization of a New Peptidomimetic Compound Modulating Sam68 Functions in Human Colon Cancer Stem Cells

Angelique Noelline Masibag

Thesis submitted to the University of Ottawa

in partial fulfillment of the requirements for

The Master of Science degree in

Cellular and Molecular Medicine

Department of Cellular and Molecular Medicine

Faculty of Medicine

University of Ottawa

uOttawa

Preface

The idea of this research project originated from Dr. Yannick Benoit. The research idea and design were cultivated by Dr. Yannick D. Benoit. The experiments were carried out under his guidance and supervision. The majority of the analysis and experiments were performed by the author.

Magnetic pull-down assay and TCGA analysis were preliminary results obtained by Dr. Yannick Benoit. CWP analogs docking analysis in PyRX and LigPlot were performed in collaboration with Francois Desrochers and Muhammad Shah. Apoptosis assay and organoid assay were performed by Chris Bergin. ChiP Assay and SRC IP were performed by Josh Haebe. The *in vivo* work was performed by the author in collaboration with Chris Bergin and Josh Haebe.

Acknowledgement

First, I wish to express my sincere gratitude to Dr. Yannick Benoit for giving me this golden opportunity to pursue my master's degree in his amazing lab. Moreover, I am very grateful that I was able to participate and learn different projects under his supervision. His continuous support and guidance made me improve and grow to a better student. Most importantly, I am very thankful for all the mentorship Dr. Benoit has given that helped me become a better researcher. I truly value all those teachings he had given me, and I will carry those learning in my future endeavours. Above all, Dr. Benoit has inspired me to become a scientist in the future.

Second, I would like to thank my advisory committee members Dr. William Stanford, Dr Jean-Francois Couture and Dr. Jocelyn Cote, for their guidance in completing my research. I am truly grateful for taking their time for reviewing my reports and presentations. With their teachings and advices, I am able to complete my research project.

Third, I would like to thank Chris Bergin (PhD Candidate) for his guidance and support throughout my master's degree. I am very grateful for all his contribution with this project by doing the Apoptosis and Serial Organoid Assays. I would also like to thank Chris Bergin and Josh Haebe (MSc candidate) for their help in *In Vivo* work. I can never ask for a better team other than you both. Also, I am truly grateful for Josh Haebe for taking his time to help me with editing my thesis and run ChIP and SRC Co-IP. I would also like to thank Franky and Muhammad for helping me out with docking. I would also like to thank Aube Morin Fournier (Co-op student) and Vanessa McGee (Honours Student) for helping me prepare samples and run my western blots.

Fourth, I would like to express my gratitude to all the members of the Benoit Lab for their encouragement and support. I am very thankful for all their constructive criticism in my reports and presentations. I am also thankful for all those exchanges of protocols and ideas that helped me honed my experiments and research. Especially thankful for Aïcha Zouggar for those long phone-calls that helped me get through the pandemic.

Fifth, I would also like to thank my friends, for their constant encouragement throughout this whole process. I am very thankful for their constant support and last minute hangouts that helped me de-stress for the whole two years of my master's journey.

Lastly, I would like to thank my parents, Noel and Evangeline, for all their moral support throughout my studies. They have given me the strength and inspiration to pursue my dreams. I am very thankful for all the things they have done that helped get to the place where I am right now. Even though they are miles away, my parents made sure that I will never miss home. Of course, I would like to thank my siblings, Alynn and Ivan for their unwavering support. Although, we are miles away, they are still my cheerleaders that kept cheering me throughout this whole process. Moreover, I am deeply grateful with my brother NJ for his support and encouragement throughout my thesis writing. Most importantly, I would like to thank my sister, Avi who has always been there for me from thick through thin. Foremost, I would like to especially thank Ryan Lee, who never stopped believing in me and never failed to make me laugh and relax on those stressful days. Overall, I am truly thankful for my family's unwavering love and support because they made it possible for me to cross the finish line.

Table of Contents

PREFACE ..... **II**

ACKNOWLEDGEMENT ..... **III**

TABLE OF CONTENTS ..... **V**

LIST OF FIGURES ..... **VIII**

LIST OF TABLES ..... **IX**

ABBREVIATIONS ..... **X**

ABSTRACT ..... **XII**

Background: ..... *xii*
Methods and Results: ..... *xiii*
Conclusion: ..... *xiv*

CHAPTER 1 ..... **1**

INTRODUCTION 1
1.1- Colorectal cancer overview *1*
1.2- Hierarchical organization of malignant cells in human colorectal tumors *3*
1.3- The canonical WNT signaling pathway represents a key therapeutic target for colorectal cancer *7*
1.4- WNT-mediated tumorigenesis as a potential anti-CSC target *9*
1.5- CBP is a transcriptional co-activator of β-catenin/TCF/LEF complexes *10*
1.6- Sam68 drives tumour progression and promotes WNT activity in CSCs *13*
1.7- Sam68 can form a complex with CBP and sequester it away from the chromatin *13*
1.8- Sam68 is a novel therapeutic target to eliminate CSCs *15*

CHAPTER 2 ..... **17**

HYPOTHESIS AND OBJECTIVES 17
2.1- Hypothesis *17*
2.2 Objectives *17*

CHAPTER 3 18

MATERIALS AND METHODS 18
3.1- Cell Culture 18
3.2- In Vitro Drug-dose Response Treatment 20
3.3- Magnetic Bead Pull-down Assay 20
3.4- Western Blot 21
3.5- Docking analysis of small molecule ligands and Sam68 P3-P5 proline-rich domains 22
3.6- Indirect Immunofluorescence 23
3.7- Half maximal effective concentration (EC50) calculation 23
3.8- Chromatin Immuno-precipitation (ChIP) 24
3.9- SRC Co-Immunoprecipitation 24
3.10- Plasmid Amplification and Purification 25
3.11- Lentiviral Sam68 and CBP Knockdown Production and Transduction 25
3.12- TCGA protein expression 26
3.13- EdU Proliferation Assay 26
3.14- Activated Caspase-3/7 apoptosis assay 26
3.15- Serial Organoid Formation Assay 27
3.16- High content cell imaging and analysis 28
3.14- RT-qPCR analysis 28
3.15- In vivo syngeneic serial tumor transplantation assays 29
3.16- Immunohistochemistry 29
3.17- Statistical Analyses 30

CHAPTER 4 33

RESULTS 33
4.1- ICG/CWP peptidomimetic compounds are direct interactors of Sam68 33
4.2- Sam68-SRC interaction is a "druggable" target in cancer 38
4.3- YB-0158 is a highly potent analog of CWP232228, disrupting Sam68-SRC interaction and reducing CBP chromatin recruitment 45
4.4- Sam68 expression mediates cancer-selective response to YB-0158 in human colorectal cancer cells 51
4.5- YB-0158 alters proliferation, apoptosis, and regulation of WNT/β-catenin targets in human colorectal cancer cells 55
4.6- YB-0158 blocks tumor-initiating capacity in primary colorectal cancer patient samples 58
4.7- YB-0158 is targeting colorectal cancer stem cell activity in vivo 62

CHAPTER 5 67

DISCUSSION 67
5.1 ICG/CWP molecules target Sam68 resulting to their anti-neoplastic effect 67
5.2 ICG/CWP molecule disrupts the SRC/Sam68 cytoplasmic interaction 68
5.3 Identification of more potent ICG/CWP class molecules is required to effectively target CSCs 69
5.4 YB-0158 effectively promotes Sam68 nuclear accumulation to disrupt transactivation of CBP/β-catenin genes 71
CHAPTER 6 75
CONCLUSION AND FUTURE DIRECTIONS 75
APPENDICES 78
REFERENCES 82

List of Figures

Figure 1. Four main stages of CRC with their respective treatments. 2

Figure 2. CRC tumours are arranged in a cellular hierarchy. 5

Figure 3. Conventional chemotherapeutics fail to target CSCs due to CSCs evasive characteristics... 6

Figure 4. The canonical WNT signalling. 12

Figure 5. ICG/CWP peptidomimetic compounds are direct interactors of Sam68 35

Figure 6. YB-0158 is a novel peptidomimetic compound predicted to bind Sam68 40

Figure 7. In Silico identification of key molecular determinants of Sam68-YB-0159 interactions 43

Figure 8. YB-0158 impacts SRC activation, Sam68 distribution, and CBP chromatin recruitment in human colorectal cancer cells..... 48

Figure 9. Sam68 expression mediates cancer-selective response to YB-0158 54

Figure 10. YB-0158 impacts proliferation, apoptosis, and expression of WNT/β-catenin target genes in human colorectal cancer cells 57

Figure 11. YB-0158 blocks tumor-initiating capacity in primary colorectal cancer patient samples . 60

Figure 12. YB-0158 is targeting colorectal cancer stem cell activity in vivo 65

Figure 13. Schematic Conclusion of Thesis. 77

List of Tables

TABLE 1. LIST OF PRIMERS USED FOR THE RT-QPCR. 31

TABLE 2. LIST OF ANTIBODIES. 32

TABLE 3. LIST OF CELL LINES AND MICE 78

TABLE 4. LIST OF CHEMICALS AND REAGENTS 79

TABLE 5. LIST OF COMMERCIAL ASSAY 80

TABLE 6. LIST OF LENTIVIRAL PLASMIDS 81

Abbreviations

5-FU	5-Fluorouracil
αSMA	α Smooth Muscle Actin
AML	Acute Myeloid Leukemia
ANOVA	Analysis of Variance
APC	Adenomatous Polyposis Coli
CBP	CREB-Binding Protein
CCSCs	Colorectal Cancer Stem Cells
ChIP	Chromatin Immunoprecipitation
CKS-α	Casein-Kinase 1α
COAD	Colon Adenocarcinoma
CRC	Colorectal Cancer
CSCs	Cancer Stem Cells
DMAP	4-Dimethylaminopyridine
E-cad	E-cadherin
FZD	Frizzled Receptor
GSK3-β	Glycogen Synthase Kinase 3 beta
IP	Immunoprecipitation
IL4	Interleukin 4
IP Injection	Intraperitoneal Injection
IR800-2-DG	IRDye-800CW-2-deoxyglucose
LRP	LDL-receptor-related protein

Oct4	Octamer-Binding Transcription Factor 4
PTDCs	Patient-Derived Cancer Cells
PDOs	Patient Derived Organoid
TCGA	The Cancer Genome Atlas
TCF/LEF	Transcription co-factor/ Lymphocytes Enhancer Binding Factor
t-hESCs	Transformed Human Embryonic Stem Cells
SUMO	Small Ubiquitin Modifier
READ	Renal Adenocarcinoma

Abstract

Background:

Conventional chemotherapeutics target bulk tumour cells and generally leave cancer stem cell (CSC) populations unaffected. Recent literature characterized the presence and the role of CSC in several types of solid tumors, including colorectal cancer. Colorectal CSCs (CCSCs) display enhanced WNT/β-catenin pathway activity, sustaining self-renewal and tumor-initiating capacity. Thus, CCSCs are crucial for tumour recurrence and metastasis. As one of the main contributors to sustained self-renewal activity in CCSCs, enhanced formation of β-catenin/CBP complex is fostering transactivation of canonical WNT target genes such as c-myc. However, maintenance of healthy intestinal stem cells also dependents on the canonical WNT pathway. Thus, selective targeting CCSCs while sparring normal intestinal cells is still a significant challenge. Interestingly, Sam68 is a key mediator of the interaction between β-catenin and CBP. It has been reported as a "druggable" target to selectively disrupt β-catenin/CBP in CSCs. Indeed, CWP232228 successfully targets CSCs in AML by facilitating Sam68/CBP complex formation, and consequently lowering the abundance of β-catenin/CBP complexes. CWP232228 was clinically tested on multiple human cancers. Unfortunately, such clinical trials were halted due to unknown causes, and limited information was released on clinical safety and benefits. Consequently, developing more potent pharmacological modulators of Sam68/CBP complex formation is still highly relevant to eradicate CCSCs. Here we describe the discovery and characterization of a new CWP

analog, known as YB-0158, which displays enhanced potency and neoplastic selectivity against CCSC.

Methods and Results:

Following the confirmation that ICG/CWP class of compounds bind to Sam68 in CSCs, I used in silico docking methods to screen for CWP analogs having high predicted affinity for Sam68 C-terminal proline-rich domain. Using high content imaging techniques, I confirmed our top candidate (YB-0158) as more potent vs. CWP parent molecule to compromise cell growth, to induce loss of pluripotency, and to increase Sam68 nuclear localization in a surrogate model of human CSCs. YB-0158 also displayed enhanced selective toxicity in colorectal cancer models vs. normal intestinal epithelium progenitor cells. Moreover, I confirmed that YB-0158 exert negative impact on cancer cell growth by inducing apoptosis and reducing proliferation. Lentiviral-based knockdowns explicitly displayed decrease in drug effectivity in the absence of Sam68, reinforcing the essential role of Sam68 mediating ICG-001/CWP response in CSCs. I demonstrated that Sam68 expression is enriched in tumor-initiating cell fractions derived from primary colorectal tumor tissues vs. bulk heterogeneous tumor organoids. Therefore, YB-0158 showed striking efficacy at supressing tumor-initiation activity in a patient-based serial organoid formation assay. Finally, YB-0158 eradicated CSCs activity *in vivo* as demonstrated by a syngeneic mouse-to-mouse serial transplantation assay.

Conclusion:

Overall, YB-0158 is a novel analog of CWP232228 with superior potency to target CCSCs activity through facilitation of Sam68 nuclear localization, thus reducing the interaction frequency between CBP and β-catenin.

Chapter 1

Introduction

1.1- Colorectal cancer overview

An uninterrupted fight against colorectal cancer (CRC) is still going on despite the great advancement in research and technology. CRC is the fourth leading cancer-related death factor world-wide and its mortality rate is expected to increase by 60% as of 2030 (Arnold et al., 2017; Brenner et al., 2014). Clinically, CRC is classified in four different stages based on tumour size and metastatic activity, which are used as guidelines for determining appropriate treatments for CRC patients (Brenner et al., 2014; Punt et al., 2017) . In the earlier stages of CRC, curative surgery is the primary intervention used to remove lesions of tumours combined with adjuvant chemotherapeutics. However, surgery is deemed to be insufficient for advanced stages of CRC yielding higher relapse rate causing for treatments to be solely dependent on conventional chemotherapeutics such as Oxaliplatin, Methotrexate, and 5-FU (**Figure 1**) (O'Connor et al., 2011; Punt et al., 2017). Yet, CRC patients in advanced stages display tumour recurrence, metastasis, and an overall low survival rate despite receiving treatments because conventional chemotherapeutics fail to target the root-source of cancer (Batlle and Clevers, 2017; Kreso and Dick, 2014; Kreso et al., 2013). This emphasizes the urgent need to develop new drugs that target the tumorigenic source of neoplastic cells for complete eradication of cancer.

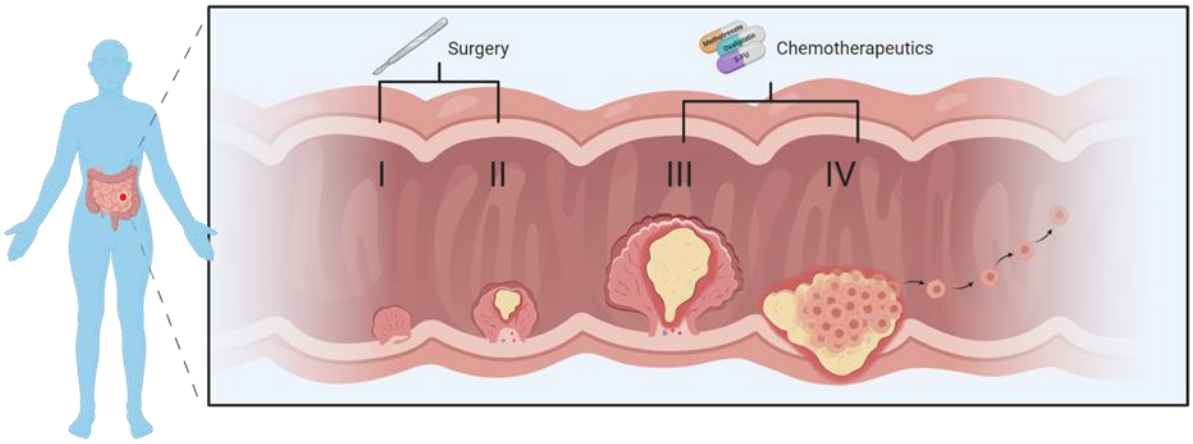

Figure 1. Four main stages of CRC with their respective treatments.

CRC are classified in four stages based on their tumour size and metastatic activity. Using these stages of CRC, clinical determination of the treatment patient will receive. Surgery remains as mainstay treatment for earlier stages of CRC, meanwhile, conventional chemotherapeutics is used for the later stages or advanced metastatic stages of CRC.

1.2- Hierarchical organization of malignant cells in human colorectal tumors

The heterogeneous nature of CRC tumours contributes to the inadequacy for conventional chemotherapeutics to target highly tumorigenic cells. The existence of cell-to-cell variations within tumours are rooted from the accumulation of genetic mutation and epigenetic alterations overtime. These oncogenic mutations and alterations create cells with phenotypic and functional diversity that are arranged in a cellular hierarchy. Similar to somatic tissues, CRC tumours are arranged in hierarchical organization that is governed by small subsets of cells, known as CSCs, with the capabilities to self-renew infinitely and initiate tumour-formation (**Figure 2**) (Gehart and Clevers, 2019; Kreso and Dick, 2014; Punt et al., 2017; Van Der Heijden and Vermeulen, 2019). These CSCs were first discovered in AML, and are identified as highly tumorigenic cells due to their capacity to repopulate tumour growth when transplanted into immune-deficient mice (Bonnet and Dick, 1997). With their unlimited self-renewal and tumour-initiating capacity, CSCs are acknowledged as the "root source of cancer", which are responsible for the high rates of tumour recurrence and metastasis associated in the advanced stages of CRC (**Figure 3**) (Batlle and Clevers, 2017; Bonnet and Dick, 1997; Joung et al., 2017; Kreso and Dick, 2014; Punt et al., 2017).

CSCs existence fuels the resistance for radiation and chemotherapeutics because of their evasive functional characteristics. The undeniable resemblance CSCs and early embryonic SCs share, from their infinite self-renewal capacity to being undifferentiated, that both cells share common transcription factor such as OCT4, a major player in pluripotency in the embryonic stem cells. In CSCs, overexpression of OCT4 is associated in maintenance of their stem-cell like properties, as

well as, increased drug resistance through increase expression of ABC transporter, which are proteins associated in chemo-resistance (Bs et al., 2015). The stem-cell like properties of CRC CSCs suggest to harbour cell surface markers associated with stemness such as CD44+, CD133+ and EpCAM distinguishing CSCs from the rest of the bulk tumour cells (Dalerba et al., 2007; O'Brien et al., 2007). Moreover, CSCs slow proliferative rate, initiation of tumour growth and resistance from apoptosis has given major advantages for CSCs survival (Batlle and Clevers, 2017; Todaro et al., 2007; Yang et al., 2020). Such that conventional chemotherapeutics target highly proliferative bulk tumour cells and often fails to target these quiescent CD133+ CRC CSCs allowing for tumour recurrence to occur (Batlle and Clevers, 2017; Todaro et al., 2007). CD133 cells have the ability to resist apoptosis through expression of IL4 (Todaro et al., 2007). However, CSCs is a rare dormant population, in fact in human CRC, CSC frequency was 1 per 5.7 x 10^4 bulk tumour cells (O'Brien et al., 2007). Their low frequency has been overlooked for the past decade as a potential therapeutic target because conventional chemotherapeutics display a more effective way of shrinking tumour mass, yet, fails to target the source of tumour recurrence and metastasis. The neoplastic capacity of CSCs highlights the importance to develop innovative chemotherapeutics specifically targeting CSCs, rather than highly proliferative bulk tumour cells, in the hope to truly extinguish this deadly disease.

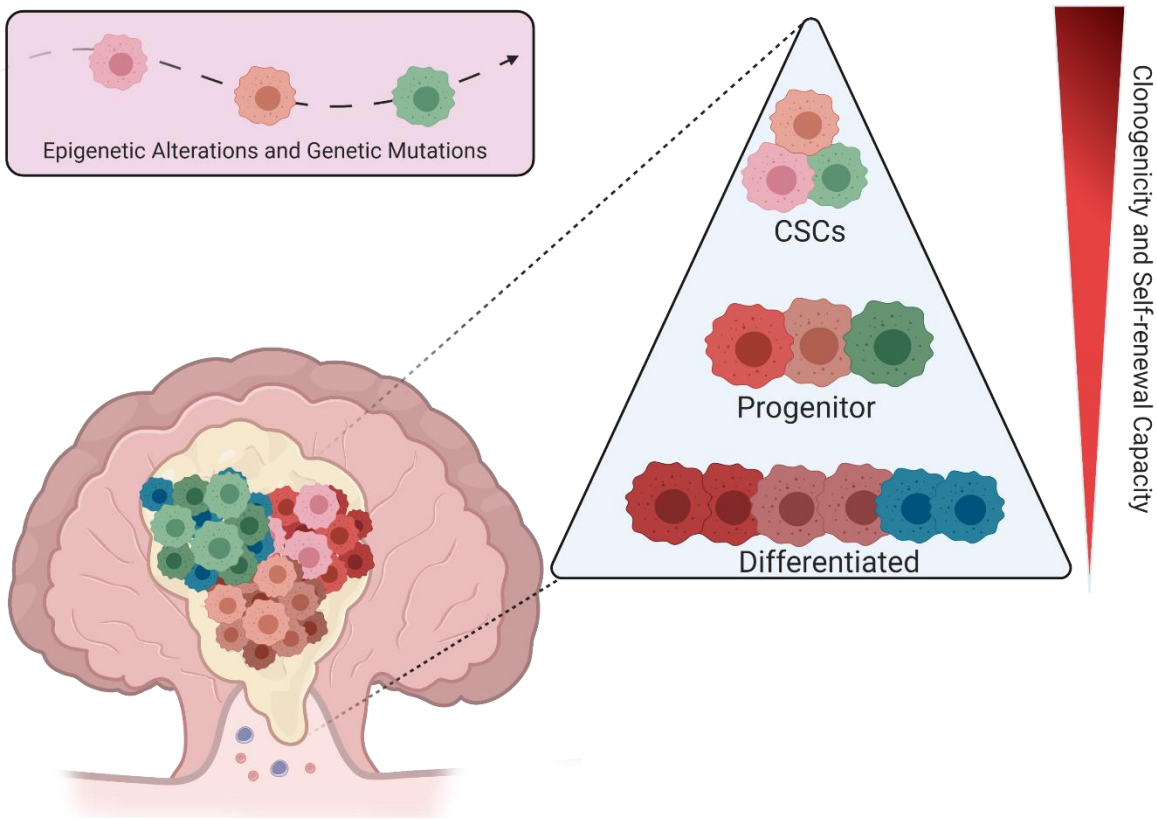

Figure 2. CRC tumours are arranged in a cellular hierarchy.

Accumulation of genetic and epigenetic mutations yield different clonal population within the bulk tumours that are arranged in a cellular hierarchical organization. Cancer stem cells (CSCs) governs the cellular hierarchy possessing the clonogenicity and self-renewal capacity.

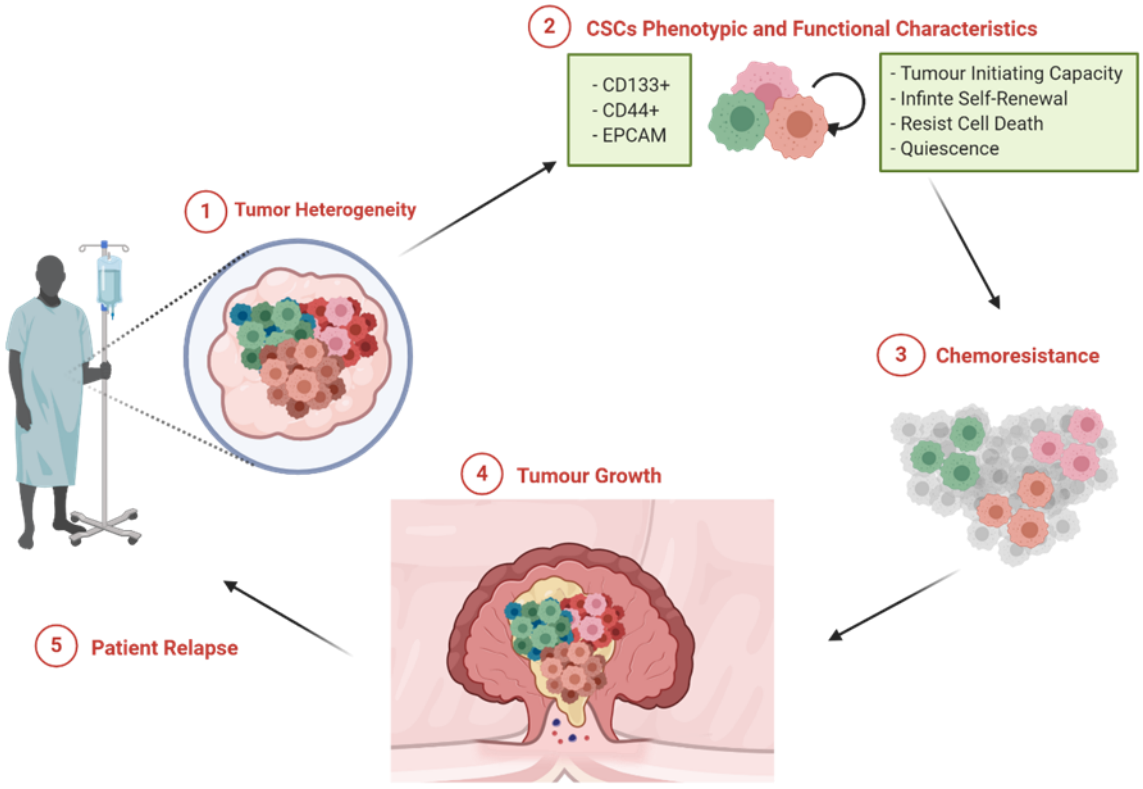

Figure 3. Conventional chemotherapeutics fail to target CSCs due to CSCs evasive characteristics.

CSCs evasive characteristics such as infinite self-renewal, tumour-initiating capacity, ability to resist cell-death, and quiescence nature give CSCs advantages to survive. The available standard chemotherapeutics target highly proliferative cells and fails to target the cells with high tumorigenic capacity leading for patient to relapse.

1.3- The canonical WNT signaling pathway represents a key therapeutic target for colorectal cancer

The development of chemotherapeutics specifically targeting CSCs has been a significant challenge for the past decade. Due to the heavy reliance of CSCs on signalling pathway such as canonical WNT signalling, Hedgehog and Notch pathways, used by somatic SCs for the maintenance of their stemness properties, it remains difficult to develop drugs exhibiting anti-CSC selectivity with limited toxicity to somatic SCs. Key proteins associated in the canonical WNT pathway, are well known to have accumulation in their genetic mutations that are linked in development of CRC (Benoit et al., 2014; Ilyas et al., 1997; Kahn, 2014; Yang et al., 2020; Zhan et al., 2017). These genetic mutations led to dysregulation of epigenetic modulators responsible for the expression of canonical WNT pathway self-renewal genes yielding evasive characteristics CSCs possess (Benoit et al., 2014). The essential role of the canonical WNT pathway in self-renewal maintenance of CSCs is a promising therapeutic target to display anti-neoplastic effect.

The highly conserved WNT signalling pathway is a critical regulator of cellular processes such as embryogenesis, tissue homeostasis, and stem cell maintenance. Within this pathway, β-catenin is the key mediator of transcriptional activity where cytoplasmic stabilization of β-catenin is tightly regulated by the “destruction complex” composed of multiple proteins. The canonical WNT pathway heavily relies on the formation and disassembly of this “destruction complex” composed of glycogen synthase kinase (GSK3-β), adenomatous polyposis coli (APC), casein kinase 1α (CSKα) and the scaffold protein AXIN. In the absence of soluble cysteine-rich glycoprotein WNT ligands, the “destruction complex” forms and mediates for phosphorylation the of β-catenin via

GSK3-β. GSK3- β phosphorylates β-catenin on ser33, ser37 and thr41 residues marking β-catenin for ubiquitination and proteasomal degradation leading to the inactivation of the canonical WNT pathway seen in **Figure** 4 (Kahn, 2014; Yang et al., 2020; Zhan et al., 2017).

In the presence of WNT ligands, WNT ligands engages with the Frizzled receptor (FZD) and LDL-receptor-related protein (LRP), activating the canonical WNT pathway. The activation of this pathway leads to a signalling cascade, in which WNT-FZD/LRP interactions facilitate for the phosphorylation of LRP via GSK3-β and CKSα. Phosphorylated LRP recruits and activates dishevelled protein (DVL) to the plasma membrane, eventually, inhibiting the "destruction complex" and β-catenin phosphorylation. Unphosphorylated β-catenin leads to increased cytoplasmic stabilization and nuclear translocation of β-catenin, which is recruited to the chromatin via its interactions with transcription co-factor/ Lymphocyte Enhancer Binding Factor (TCF/LEF). Despite tight regulation of β-catenin, recruitment of transcriptional co-activator such as CREB-binding protein (CBP)/P300, are subsequently recruited to potentiate the transactivation of canonical WNT target genes, such as *c-myc*, that are highly involved in stem-cell like property maintenance (Figure 4) (Kahn, 2014; Yang et al., 2020; Zhan et al., 2017). Subsequently, recruitment of β-catenin to the TCF/LEF binding domain is highly involved in the expression of key pluripotency markers such as OCT4, Nanog and Sox2. Conversely, WNT/ β-catenin pathway controls the ability for ESCs to commit to distinct cell lineages (Sokol, 2011). Furthermore, the tight regulation of β-catenin plays an essential role in preserving the structural integrity and homeostasis for both small intestines and colon through the maintenance of the intestinal SCs at the bottom of the crypt. There is significant accumulation of β-catenin seen in cells found in the intestinal and colonic crypts (Pinto et al., 2003; Van De Wetering et al., 2002). In fact, that

complete ablation of β-catenin led to a complete disruption of intestinal crypt architecture and integrity (Fevr et al., 2007). Moreover, aberrant nuclear accumulation of β-catenin is directly, linked to the development of CRC due to the uncontrollable self-renewal ability of intestinal SCs, thus, leading to the emergence of CSCs (Van De Wetering et al., 2002).

1.4- WNT-mediated tumorigenesis as a potential anti-CSC target

The WNT pathway is critical regulator of stem cell pluripotency that any discrepancy in the pathway can lead to the development of CSCs. Since WNT/β-catenin is regulated by multiple proteins, there is vast potential for dysregulation to occur. For instance, in CRC, mutation in APC in prevalent, in which APC fails to act as scaffold for the "destruction complex", thus, destabilizing the "destruction complex" and failing to regulate β-catenin proteasomal degradation (Zhan et al., 2017). As a consequence, increased nuclear β-catenin occurs leading to increased expression of stem-cell-associated WNT genes (Kahn, 2014; Yang et al., 2020; Zhan et al., 2017). In another instance, mutations on the β-catenin gene, *CTNBB1,* alters β-catenin functional ability (Behrens and Lustig, 2004; Ilyas et al., 1997). In a study conducted by Ilyas and colleagues highlighted β-catenin mutations across 23 CRC cell lines (Ilyas et al., 1997). Specific mutations on *CTNBB1* allows for increased nuclear formation of β-catenin/TCF-LEF complex and its transcriptional-related activity (Behrens and Lustig, 2004; Ilyas et al., 1997). Upregulation of β-catenin/TCF-LEF mediated the stem-cell-associated WNT genes, which may potentially promote tumorigenesis (Behrens and Lustig, 2004; Vermeulen et al., 2010). Both hyperactivated WNT/ β-catenin activity and increased nuclear accumulation of β-catenin were correlated to poor prognosis in CRC (Chen et

al., 2013; Kahn, 2014). Dysregulation in the upstream protein regulators of WNT/ β-catenin may occur in different mechanisms, there is still the common denominator of increased expression of genes associate with stem-cell like properties allowing for the long-term maintenance of CSCs. Therefore, it is important to develop chemotherapeutics that limits the expression of β-catenin/TCF/LEF mediated genes without jeopardizing homeostasis regulation of somatic SCs.

1.5- CBP is a transcriptional co-activator of β-catenin/TCF/LEF complexes

An interesting therapeutic avenue to target CSCs whilst sparring somatic SCs is through targeting the downstream regulator of the canonical WNT pathway. Critically, β-catenin have a broad network of interactions with different transcription factors essential for the downstream cellular processes such as pluripotency and oxidative stress (Kahn, 2014). Hence, inhibition of β-catenin may posit detrimental cellular effects, thus, this needs to be considered in development of therapeutics targeting the canonical WNT pathway.

Since CSCs rely heavily in epigenetic alterations that gives them functional advantages. Notably, WNT/ β-catenin pathway is associated with the epigenetic alterations such as modulation in histone acetylation that is prevalently seen in cancer progression. Such that changes in histone acetylation is related with the enhanced activity of CBP/p300 (Benoit et al., 2017). CBP/p300 is a promising therapeutic avenue to explore since CBP is highly involved in the transactivation of β-catenin/TCF/LEF self-renewal associated genes such as *c-myc, CD44, survivin,* and *sox4* (Benoit et al., 2014; Kahn, 2014; Ma et al., 2005; Miyabayashi et al., 2007a). Meanwhile, p300 is mainly

involved in differentiation processes (Kahn, 2014). CBP/p300 is equipped with histone acetyltransferase domain (HAT) responsible for the acetylation of the histone tails, resulting to the neutralization of the positively charged histone protein and the negatively charged DNA promotes chromatin unwinding and increased transcriptional activity (Chan and La Thangue, 2001). The transcriptional activity of CBP is directly targetable, either through the inhibition of CBP/p300's HAT activity or disrupting CBP/β-catenin interaction. The development of C646, a small molecule capable of inhibiting the HAT activity specifically in p300 leads to a decrease in overall histone-3 (H3) acetylation and ultimately a decrease with the associated of β-catenin transactivation displaying anti-neoplastic effects (Benoit et al., 2014; Bowers et al., 2010; Santer et al., 2011). The discovery of ICG-001, which inhibits the interaction between CBP and of β-catenin through binding to CBP, thereby downregulating β-catenin/TCF/LEF transactivation (Emami et al., 2004). A second generation inhibitor of CBP/β-catenin and a more potent ICG-001 analogue, PRI-724, displayed a more successful phase1a/1b clinical trial, with its toxicity within the acceptable range (Lenz and Kahn, 2014). Although these small molecules are alleged to inhibit the interaction between CBP/β-catenin complex, with great specificity for CSCs, little is known about their exact mechanism of action (Benoit et al., 2014; Emami et al., 2004; Lenz and Kahn, 2014). Therefore, identifying unique cellular property of CSCs, that can be harnessed to selectively target CSCs, but not somatic SCs, will be a great way to facilitate for the development of small molecules specifically targeting CSCs.

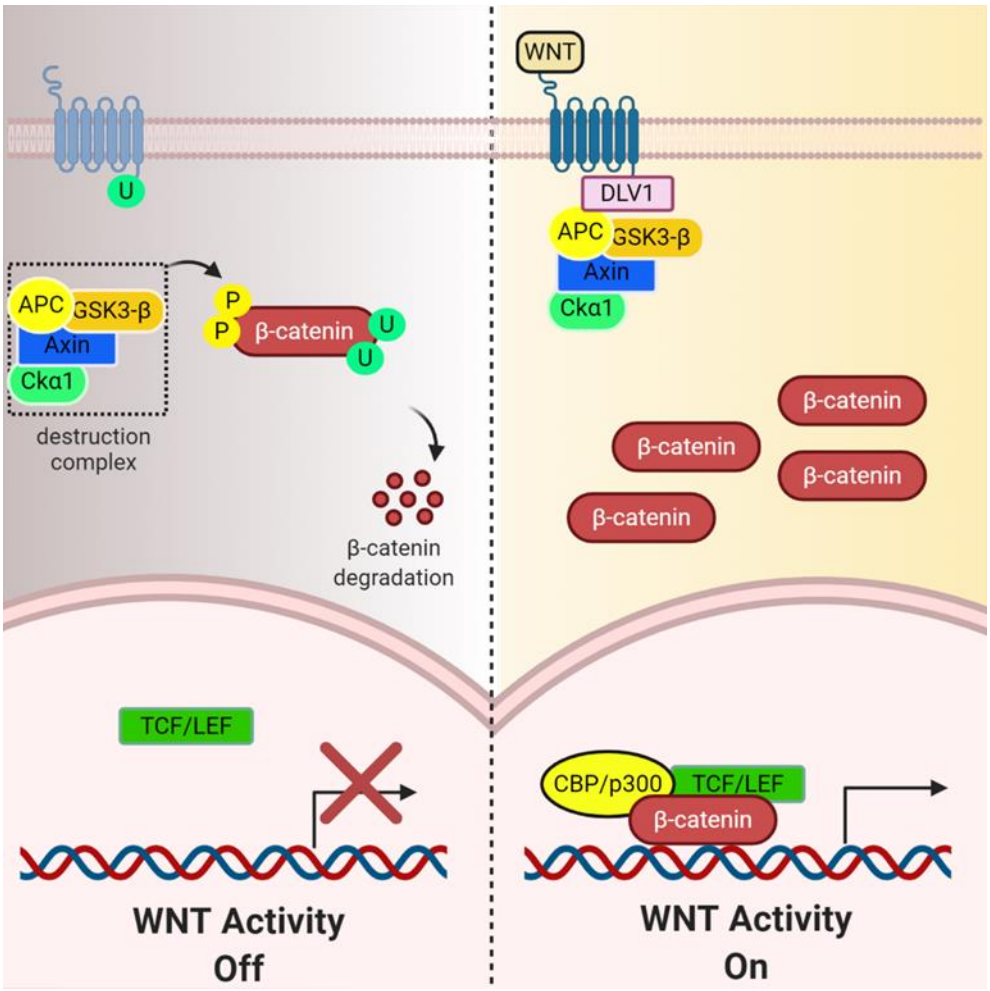

Figure 4. The canonical WNT signalling.

The canonical WNT pathway plays a role in cellular homeostasis and stem cell maintenance. In the absence of WNT ligand the destruction complex marks β-catenin for degradation. Upon degradation of β-catenin, the WNT activity is turned off. Meanwhile, in the presence of WNT ligand, de-activated the destruction complex. This has led for stabilization of cytoplasmic β-catenin, which is then translocated into the nucleus. Nuclear β-catenin recruits transcription factors, thus activating WNT activity allowing for WNT gene transcription to occur.

1.6- Sam68 drives tumour progression and promotes WNT activity in CSCs

While CBP is not displaying the expression specificity, required for an effective anti-CSCs treatment, CBP does not work alone when mediating gene transactivation. Critically, CBP co-regulators play an important role in directing the recruitment of CBP / β-catenin target gene promoters. One such regulator, SRC-associated in mitosis 68kDa (SAM68), plays critical roles in transcription factor organization, post-transcriptional RNA regulation as well as various cytoplasmic roles as a messenger molecule. Functionally, SAM68 is quite promiscuous, interacting with various signalling pathways, both in the nucleus and cytoplasm (Bielli et al., 2011; Frisone et al., 2015). However, upregulated levels of Sam68 is seen in different types of cancer and is correlated in tumour progression (Busà et al., 2007; Lukong and Richard, 2007; Song et al., 2010). Sam68 has first been identified as an interactor with the tyrosine kinase phosphatase c-SRC during mitosis (Taylor et al., 1995). During mitosis, c-SRC is highly active in which, dephosphorylation occurs in Tyr-527 to phosphorylate SH2 and SH3 domain of Sam68 resulting in modulation in its RNA binding capacity (Taylor et al., 1995). In cancer, it has been noted that increase SRC activity displays a link in tumour progression and cellular proliferation (Resh, 2008).

1.7- Sam68 can form a complex with CBP and sequester it away from the chromatin

In another instance, Sam68 interacts with CBP, which might involve the phosphorylation of the tyrosine rich domain of Sam68. However, this is still an unknown phenomena (Hong et al., 2002b). The KH domain of Sam68 containing FXD/EXXXL motif interacts with the CH3 domain of

CBP. In fact, The CH3 binding domain of CBP is known to interact with multiple nuclear binding factors such as p53, GATA-1 and β-catenin (Freedman et al., 2002; Takemaru and Moon, 2000). Sam68 competes with other nuclear binding factors for CBP. The interaction between Sam68 and CBP allows for Sam68 to dislodge GATA-1 from the CH3 domain of CBP (Hong et al., 2002b). In addition, Sam68 has a transcriptional repression ability outside its RNA binding (Hong et al., 2002b). Therefore, Sam68 represses the transcriptional activity of CBP upon their interaction (Hong et al., 2002b). Overall, Sam68/CBP complex may display anti-neoplastic effect.

Since CBP has an acetyltransferase activity, CBP may influence the activity of Sam68. Acetylation of Sam68 influences its ability to bind to poly-U-RNA (Babic et al., 2004). However, Babic and colleagues also argues that Sam68 is acetylated by multiple other protein and not just CBP at all. In their study, they disclosed that at low levels of CBP's HAT activity, Sam68 acetylation in cancer cell lines were still elevated (Babic et al., 2004). Thus, CBP acetylation in Sam68 may be independent on its ability to bind to poly-U-RNA.

Interestingly, localization of Sam68 may play a role in the progression of cancer. Evidences have shown upregulated levels of Sam68 is seen in multiple types of cancer (Benoit et al., 2017; Bielli et al., 2011; Sumithra et al., 2019). Similarly, Sam68 is highly expressed in t-hESCs (transformed human embryonic stem cells) (Benoit et al., 2017). Cytoplasmic localization of Sam68 correlated with poor prognosis of renal cancer¸ breast cancer, and cervical cancer (Frisone et al., 2015; Zhang et al., 2009). In addition, Sam68 enrichment in the cytoplasm has been seen to promote lymph node metastasis (Frisone et al., 2015). Thus, these evidences laid out indicate that Sam68 cytoplasmic localization promotes tumour progression and metastasis. Meanwhile, a study displayed that nuclear localization of Sam68 inverses the tumour progression effects that

cytoplasmic Sam68 holds (Benoit et al., 2017). This suggest that Sam68 nuclear localization can potentially inverse the effects of upregulated levels of Sam68 in the cytoplasm.

1.8- Sam68 is a novel therapeutic target to eliminate CSCs

CBP and Sam68 interaction evidently occur only in cancer cells, along with t-hESCs, specifically in CSCs (Benoit et al., 2017; Hong et al., 2002b). Since Sam68 possess the ability to repress transcription, Sam68 is an appealing therapeutic target to eradicate cancer. ICG/CWP molecule is known to disrupt the interaction between CBP and β-catenin to halt WNT activity (Benoit et al., 2017; Emami et al., 2004). CWP 232228 promotes Sam68 nuclear localization in t-hESCs, AML, breast and colorectal cancer cells (Benoit et al., 2017; Jang et al., 2015). This in turns allows Sam68 to disrupt the interaction between CBP and β-catenin. This displaying anti-neoplastic effect. However, CWP molecular mechanism of action is still unknown. Benoit and colleagues disclosed that Sam68 undergoes SUMOylation, which is a post-translational modification, as a consequence of the drug treatment. Moreover, SUMOylation seems to play a role in the localization of Sam68 (Benoit et al., 2017). Although further studies are still required to fully understand CWP mechanism of action and its role in the localization of Sam68. What we know so far is that CWP shifts the enrichment of Sam68 from cytoplasm to nucleus which allows for Sam68 interact with CBP and outcompetes β-catenin, which results to inhibiting the transcription of self-renewal genes (Benoit et al., 2017).

Most ICG/CWP molecules stopped at the phase 1A/1B clinical trials due to its adverse effects and with not much information disclosed (Ko et al., 2016). Therefore, finding a new treatment targeting Sam68 is very important, especially up to this date there are little known small molecules targeting Sam68. One is the small molecule, UCS15A targeting the proline rich region of Sam68. USC15A binds to the proline rich domain of Sam68 to disrupt its interaction with c-SRC (Oneyama et al., 2002). With this knowledge, Sam68 proline rich domain is a great target to identify binding of new molecules.

We proposed that by identifying CWP analog possessing greater potency than CWP228 targeting Sam68 will promote anti-neoplastic effect. Through identifying new CWP derivatives that binds to Sam68 proline-rich domain, CWP will disrupt the cytoplasmic interaction of SAM68 and c-SRC. Consequently, allowing for Sam68 to be free to be translocated into the nucleus. We proposed that Sam68 nuclear enrichment disrupts CBP/ β-catenin interaction through outcompeting β-catenin binding to CBP's CH3 domain. This will inhibit the canonical WNT pathway. Through facilitating Sam68 localization allows to selectively target CSCs without jeopardizing the normal healthy stem cells. This project explores a novel small molecule, YB-0158, which effectively targets CSCs *in vitro*, and *in vivo*.

Chapter 2

Hypothesis and Objectives

2.1- Hypothesis

YB-0158 is a novel peptidomimetic compound (ICG/CWP analog) which interacts with Sam68 to inhibit the canonical WNT pathway and tumour-initiating capacity in human colon cancer stem cells (CCSCs).

2.2 Objectives

Objective 1: Identifying key interactors of ICG/CWP molecules and its role in ICG/CWP effectivity

Objective 2: Identification of a more potent ICG/CWP analog interacting with Sam68 and potentially exhibiting anti-neoplastic effects.

Objective 3: Confirming the molecular mechanism of YB-0158 in colorectal cancer

Objective-4: To demonstrate the efficacy of YB-0158 at supressing cancer stem cell activity *in vivo* using a syngeneic serial tumor transplantation model

Objective-5: To characterize the efficacy of YB-0158 at suppressing tumour-initiating capacity in human patients-derived colorectal cancer specimens

Chapter 3

Materials and Methods

3.1- Cell Culture

HIEC Cell Culture

The normal intestinal epithelium cell line, HIEC, were cultured in Opti-MEM Reduced Serum with 1% Hepes and 1% L-glutamine mixed with 5% Wisent Premium and 10 ng/mL Epithelial Growth Factor. The cells were cultured at 10 mm culture plate at 37 °C 5% CO_2. The media were changed every 3 days. The cells were passed every 5 days at a 1:3 ratio.

HT29 Cell Culture

The human colorectal adenoma cancer cell line, HT29 (female), were cultured in McCoy's 5A Medium with L-Glutamine mixed with 10% Fetal Bovine Serum. The cells were cultured at 10 mm culture plate at 37 °C 5% CO_2. The cells were pass every 5 days in 1:10 ratio and the media were changed 3 days after passage.

HCT116 Cell Culture

The human colorectal adenoma cancer cell line, HCT116 (male), were cultured in McCoy's 5A Medium with L-Glutamine mixed with 10% Fetal Bovine Serum. The cells were cultured at 10 mm

culture plate at 37 °C 5% CO_2. The cells were passed every 5 days in 1:10 ratio and the media were changed 3 days after passage.

MC-38 Cell Culture

The C57BL6 murine colorectal adenoma cancer cell line, MC38, were cultured in DMEM/High Glucose (HyClone) with 4 mM L-Glutamine, 4500 mg/L Glucose, and sodium pyruvate mixed with 10 % Fetal Bovine Serum at 37 °C 5% CO_2. The cells were passed every 5 days in 1:10 ratio and the media were changed 3 days after the passage.

t-hESCs (v1H9) Cell Culture

The transformed pluripotent stem cells (t-hESCs) v1H9 were cultured in mTSER medium with mTSER supplement in a 6 well-plate coated with Matrigel at 37 °C 5% CO_2. The medium was changed the day after the cells were passed. The cells were passed in 1: 5 every 5 days using 1X Collagenase IV in clumps through scraping of the cell surface.

Primary Colorectal Tumour Patient Samples Culture

Three patient samples (92,162,146) were cultured in DMEM/F12 1:1 (Gibco) with supplements of 1% Pen/Strep, 1x Non-essential amino acids, 1x Hepes, 4ug/mL Heparin, 1mL of lipids, 20ng/mL EGF, 10ng/mL bFGF, N2 and B27 supplements, 1 mM Sodium Pyruvate and 2mM L-

glutamine at 37 °C 5% CO_2. The media are changed every 7 days and the spheres are passed once a week.

3.2- *In Vitro* Drug-dose Response Treatment

The drug-dose response was performed by seeding 10 000 cells of HIEC, 5 000 cells of HT29, 5 000 cells of HCT116, 5 000 cells of MC38 and 10 000 cells of v1H9 (t-hESCs) in their respective 96 well plates. After 24 hours of seeding, the cells were treated with 1% DMSO (control) along with drug dose between 0.04 µM to 10.00 µM of PRI-724, CWP232228 and YB-0158. The cells were treated for 48 hours at 37 °C 5% CO_2. After 48 hours of drug treatment, the cells were washed with 1X PBS and fixed with 4% paraformaldehyde for 20 minutes.

3.3- Magnetic Bead Pull-down Assay

Human pluripotent cells were lysed in 1% NP-40 lysis buffer (50 mM Tris-HCL pH 7.4 + protease inhibitor cocktail) and quantified. Suspensions of 0.8mg of total protein content were incubated with CWP232904-conjugated magnetic Dynabeads (BioSynthesis Inc, TX.). Unconjugated magnetic Dynabeads were used as control matrix. 100uM of soluble CWP and ICG-001 were added to the mixtures for competition assays. Samples were incubated for 2h at room temperature under agitation and were washed 3 times using 1% NP-40 lysis buffer + protease inhibitor cocktail. Washed beads were boiled in Laemmli sample buffer at 95°C for 10 min and analyzed by Western blot as elaborated in Section 3.4.

3.4- Western Blot

Total protein samples were prepared in 4X Laemmli Buffer (0.1% β -Mercaptoethanol, 10% Glycerol, 0.005% Bromophenol Blue, 62.5mM Tris-HCl pH 6.8, and 1% SDS) and sonicated (30% amplitude 5 second pulses and 3 second rest). Total protein concentration was quantified through dot blot. Prior to running the western blot, the total protein samples were denatured in 95 ºC for 5 min. The Marker GE Amersham ECL Full-Range Rainbow Ladder (VWR) and samples were run in a 10 % and 12.5 % polyacrylamide gels. After protein migration and transfer, the non-specific proteins were blocked with 5% skimmed milk in 1X PBS 0.1% Tween-20 for 30 minutes followed by its respective primary antibody incubation, diluted in blocking buffer in 4 C overnight. Followed by an additional primary antibody incubation for 1 hour at room temperature. After the primary antibody incubation, the membranes were washed with 1X PBS 0.1% Tween-20 for 3 sequential washes. The membranes were incubated in horseradish peroxidase-conjugated secondary antibodies which was diluted in 1X PBS 0.1% Tween for 1 hour at room temperature. This is followed by 3 consecutive washes with 1X PBS 0.1% Tween. Visualization of the membranes were done by addition of Immobilon Western Kit. Images were taken using ChemiDoc MP Imaging System (Bio rad). The blots were quantified using Image J software (National Institutes of Health).

3.5- Docking analysis of small molecule ligands and Sam68 P3-P5 proline-rich domains

171 CWP-analog structures were docked into the P3-P5 proline-rich regions of Sam68, which are regions known for interaction with the small molecule UCS15A (Oneyama et al., 2002). As an initial step, Sam68's P3 to P5 region (amino acid 275 to 305) to structural regions were obtained through the use of TASSER-VMT algorithm (Zhou and Skolnick, 2012). While, the generated SMILES of drug compounds were used to build compound structure in Chimera. Sam68 protein structures and ligands were prepared into pdbqt files using PyRX ensuring that proteins contained each atom's respective hydrogens and water molecules were discarded (Dallakyan and Olson, 2015). Subsequently, protein-ligand docking was performed by assigning each compound with an X-score using Autodock Vina. Autodock Vina scoring considered the gaussian steric interaction, finite repulsion, piecewise linear hydrophobic, entropic term and hydrogen bond interaction between the protein and the ligand (Gaillard, 2018; Trott and Olson, 2010) with an assumption of the receptor as a rigid protein while compounds are flexible molecules with a range of 0 to 32 active rotatable bonds (Forli et al., 2016; Trott and Olson, 2010). Once the proteins and ligands were both ready for docking, using PyRx, Autodock Vina was run. Each run used an exhaustiveness of 50 in triplicates. Each compound docked to the receptor were given a score (ΔG) based on the intermolecular and intramolecular total contribution and ranked (Trott and Olson, 2010). The predictive binding energy was calculated using **Equation 1**. Validation of protein-ligand interactions and visualization of main residues putatively involved were performed using LigPlot and Chimera (Laskowski and Swindells, 2011).

$$K_{eq} = 10^{-\Delta G/1.36}$$

Equation 1. Predictive binding affinity score equation.

3.6- Indirect Immunofluorescence

Experimental samples were prepared in 96-well plates, as described in Method Section 3.2. Immunofluorescence was performed to observe OCT4, and FOXA2 expression and Sam68 nuclear localization in t-hESCs and HT29. As the initial steps for immunofluorescence staining, cells were washed with 1X Perm wash followed by primary antibody incubation overnight at 4ºC. Each antibody was used for its respective experiments; for OCT4 fluorescence, primary anti-OCT4, FOXA2 fluorescence, primary anti-FOXA2, while Sam68 fluorescence, primary anti-Sam68 listed in Table 2. After primary antibody incubation, cells were washed with 1X Perm wash and incubated with their respective secondary antibody, Alexa Fluor 488 listed in Table 2, at room temperature for 1 hour. Nuclei staining was done using Hoechst for 10 minutes at room temperature.

3.7- Half maximal effective concentration (EC50) calculation

Obtained cell counts based from Method Section 3.2 were plotted and calculated from AATBioquest (www.aatbio.com).

3.8- Chromatin Immuno-precipitation (ChIP)

HT29 Cell plating and treatment were performed as elaborated in Method Section 3.1 and 3.2. ChIP assay was performed for CBP binding target as described in described in Benoit *et al.* (2017). After 48-hour cell treatment, the cells were cross-linked using 0.1% PFA, harvested and sonicated to get DNA fragments of ~250bp. Size of the fragmented DNA-bound protein were verified using 1% Agarose gel electrophoresis and incubated overnight at 4 ^{o}C with Protein G magnetic Dynabeads with the respective mouse anti-CBP or anti-IgG antibodies (see Table 2). Afterwards, the beads were initially washed with IP buffer and protease inhibitor cocktail followed by reverse cross-linking. The DNA fragments are purified following the Chromatin IP Purification Kit manufacturer's protocol. The DNA fragments were measured by qPCR elaborated in Method Section 3.14 (see Table 1 for promoter target gene primers).

3.9- SRC Co-Immunoprecipitation

HT29 Cell plating and treatment were performed as elaborated in Method Section 3.1 and 3.2. Cells were lysed using lysis buffer containing 50mM Tris-HCl pH 6.8, 150mM NaCl, 2mM EDTA pH 8.0, 1% NP-40, (pH to 7.4) for 30 minutes at 4 ^{o}C. Proteins were collected through centrifugation at 12 000 rpm for 20 minutes. Afterwards, proteins were incubated with Protein G magnetic Dynabeads for 1 hour at room temperature, followed by incubation with v-SRC and IgG conjugated beads overnight 4 ^{o}C. The conjugated proteins were washed and the proteins were eluted using Laemmle+5%BM at 65 ^{o}C. for 10 minutes. The samples were validated and analysed by western blot elaborated in Method Section 3.4.

3.10- Plasmid Amplification and Purification

Bacterial samples harbouring the CBP and Sam68 knockdowns were inoculated overnight in LB Broth at 37 ºC with continuous shaking. After inoculation, the bacterial samples were purified using QIAprep spin Miniprep kit. To verify the purity of lentiviral plasmids, obtained lentiviral plasmids were ran in 2% Agarose gel for 1 hour.

3.11- Lentiviral Sam68 and CBP Knockdown Production and Transduction

Sam68 and CBP lentiviral particles for knockdowns were generated through transfection of HEK cells using packaging vectors pMD2.G and psPAX2, and Sam68 and CBP respective plasmids shCLNG listed on Table A .5 Transfection medium were prepared using 15 µL of Lipofectamine LTX reagent (Invitrogen) mixed with 3.5 µg of vectors in OptiMEM Free medium (Gibco). Once HEK293-FT cells reached 70% confluency the cells were transfected with transfection medium (added drop-wise) and incubated for 1 hour at 37 ºC 5% CO2 followed by the addition of 2 mL 10% FBS DMEM/High Glucose Media. Medium was changed after overnight incubation. After 48 hours of transfections, lentiviral particles were collected using a syringe and filtered through 45 µM filter syringes. The collected lentiviral were used to transduce HT29 cells to create a stable Sam68 and CBP knockdown cell lines. HT29 cells were transduced with lentiviral particles using 8 ug/mL of polybrene mixed with 10% FBS McCoy medium. The mixtures were added dropwise to 60 to 70 % confluent HT29 cells. 250 µL of lentiviral particles were added to each respective well and incubated overnight followed by the change of medium the next day. After 48 hours of

transduction, HT29 cells were subjected to 2.5 ug/mL of puromycin selection for 10 days. Validation of the knockdowns was done by Western Blot (see Method Section 3.4).

3.12- TCGA protein expression

Transcript expression of WNT transcriptional activators were extracted from the Cancer Genome Atlas (TCGA) colonic adenocarcinoma (COAD) and rectal adenocarcinoma (READ) vs normal patients. Extracted data were plotted using http://gepia2.cancer-pku.cn/#index (Tang et al., 2019).

3.13- EdU Proliferation Assay

HT29 cells were seeded at 5 000 cells in a 96 well-plate. After 24 hours of seeding, the media were changed to McCoy's 5A medium (Lonza) without serum and incubated for another 24 hours at 37 °C 5% CO_2. After 24 hours of cell starvation, they were treated with 1% DMSO (control), 0.2 µM and 0.5 µM of CWP232228 and YB-0158, and 1.25 µM of Chiron (positive control). The proliferation assay was performed by following the procedure in the EdU proliferation kit (Abcam, Cat# ab222421). All cells were stained with Hoechst as a nuclear stain. Cell visualization and quantification of % EdU positive cells was performed as described in the Method Section 3.13.

3.14- Activated Caspase-3/7 apoptosis assay

Five thousand HT29 cells were initially seeded on a 96 well-plate. 24 hours after plating, the cells were treated with 0.2 µM and 0.5 µM YB-0158, 1% DMSO (negative control) for 48 hours. Before

starting the assay, 1 µM staurosporine was added to additional wells and served as a positive control and an inducer of apoptosis for 6 hours. After 6-hour of incubation, all the cells were stained using the CellEvent Caspase-3/7 assay kit by following the manufacturer's protocol at a final concentration of 5 µM. All cells were stained with Hoechst as a nuclear stain. Cell visualization and quantification of % positive Caspase3/7 were performed following the Method Section 3.13.

3.15- Serial Organoid Formation Assay

Assessment of drugs efficacy on targeting the tumour-initiating cells were performed through serial clonogenic assay (Rizo et al., 2008). Patient samples were derived from dissociated patient tumour using 1X Collagenase and collected to perform a serial organoid assay. Extracted patient samples were run in ultra-low adhesion culture conditions to form spheroids, which are enriched with CSCs. Spheres were dissociated into single cells using 1x TrypLE Express through mechanical pipetting and they were filtered from cell aggregates using 70-µm strainer. 300 Single cells were collected and mixed with Matrigel in 1:1 ratio in spheroid culturing media. The cell-Matrigel mixture were plated in a 6 well-plate in a dome formation at a 1cell/uL cell density, which was let to solidify at 37 ºC for 15 minutes. After dome formation, each well was supplemented with spheroid culturing media mixed with its respective dose of YB-0158 (0.0165 µM to 2 µM) vs 0.1% DMSO (control) and incubated for 7 days at 37 ºC 5% CO2. After 7 days of incubation, the spheroid media with drugs were removed from the domes and a fresh drug-free spheroid media were added and incubated for another 7 days. This is followed by organoid imaging and organoid count using Cellomics Array Scan VTI (Thermofisher). Afterwards, each drug treated primary

organoids dome were dissociated into single cells with Dissociation Reagent. The single cells were mixed with Matrigel in 1:1 ratio in spheroid culturing media and 15 000 cells/well were plated. The cell-matrigel mixture was let to solidify at 37 ºC for 15 minutes. Each dome was added with drug-free spheroid culturing media and it was incubated for 14 days at 37 ºC 5% CO2. Organoid images and counts were taken using the Cellomics Array Scan VTI (Thermofisher), see Method Section 3.16.

3.16- High content cell imaging and analysis

Visualization of cell counts, immunofluorescence and organoid counts were performed using Cellomics Array Scan VTI (Thermofisher) from Stem Core Laboratory at the General Ottawa Hospital. Analysis and quantifications were done using HCS StudioTM Software.

3.14- RT-qPCR analysis

Total RNA was extracted and purified using RNeasy Mini Kit (Qiagen) by following the manufacturer's protocol. Quantification of purified RNA were performed using Nanodrop 2000 Spectrophotometer (Thermo Scientific). cDNA synthesis was done using 500 ng of purified RNA and Superscript III FirstStrand Synthesis (Life Technologies) followed by running samples in Thermocycler (Thermofisher). The synthesized cDNA was mixed with PowerSybr Green PCR master mix (Life Science) and its corresponding primers seen in Table 1. The RT-qpcr were ran in ABI 7500 Real-Time PCR system (Applied Biosystems). All data were normalized to GAPDH and fold changes were calculated based on the method described by Pfaffl in *Nucleic Acids Res* (Pfaffl, 2001).

3.15- *In vivo* syngeneic serial tumor transplantation assays

Assessment of drug capacity to target the function of cancer stem cells were performed using *in vivo* xenograft assay. MC38 cells were prepared in 1:1 HBSS:Matrigel coating prior to injection. MC38 cells were injected into the left and right flanks of the primary C57/BL6 female recipient mice (6 to 8 weeks old) at a density of 1 x 10^{6} MC38 Matrigel-coated cells per site. Engraftment lasted for 7 days. Subsequently, 100mg/kg of YB-0158 (n=4) or CWP232228 (n=4) vs. control saline (HBSS vehicle) (n=5) was intraperitoneally injected for 14 days. The tumour growth was measured in two dimensions using a digital caliper for 11 days straight and after tumour extraction, which is used to calculate ellipsoidal tumour volume. The ellipsoidal tumour volume formula used is ½ * (Length * $Width^2$). The primary tumours were extracted, dissociated, re-suspended, and coated with Matrigel. The primary tumour cells (500 000 and 1 x 10^{6}) were re-injected subcutaneously in the left and right dorsal flank and both shoulders respectively. The tumours were left to engraft for 14 days without treatment. Afterwards, the mice were sacrificed, and tumours were extracted and measured. The University of Ottawa Animal Care Facility approved the protocol elaborated in this procedure.

3.16- Immunohistochemistry

Small intestine dissected from primary mice were clean flushed with 1X PBS followed by 10% buffered formalin fixation for 72 hours at 4 C. Fixation were stopped with 70% ethanol and the samples were sent to Louise Pelletier Histology Core Facility at the University of Ottawa for sectioning, paraffinization, de-paraffinization, and antigen retrieval. The tissue samples were

sectioned in 4 microns and embedded on microscope tissue slides. Each tissue samples were quenched with 1.25% glycine solution for 30 minutes at room temperature. The slides were blocked with 2% BSA at room temperature for 30 minutes. Primary mouse anti-ki67 (Biogen) has been used to assess proliferation in the intestinal crypt. Meanwhile, primary mouse monoclonal anti-smooth muscle actin (SMA) (R&D system) and primary anti-E-cadherin antibody were used to assess the mucosae architecture of the intestine. The respective slides were incubated overnight at 4 ºC followed by consecutive washes on 1X PBS. The slides were incubated with their respective secondary antibodies Alexa Fluora 555 and Alexa Fluora 488 (Table A3) for one hour at room temperature. At the end of the one-hour incubation, the slides were washed three consecutive times for 15 minutes with PBS. The preservation of fluorescence and prevention of photobleaching were done by addition of Vectashield Antifade Mounting Medium (Vectashield). Nuclei staining were done with Dapi included in the Vectashield Antifade Mounting Medium (Vectashield). Images were taken using Zeiss AxioImager M2 at the Cell Microscopy core of University of Ottawa.

3.17- Statistical Analyses

Data are all represented as a ±SEM. The statistical analysis was all performed using GraphPad Prism 8 software. One-way ANOVA were used to compare the different experimental groups to control in *in vitro* drug treatment, immunofluorescence, proliferation and apoptosis assay, and serial organoid assay. Unpaired t-test were used for RT-qPCR analysis. Meanwhile, *in vivo* xenograft assay used fisher exact test, followed by a post hoc analysis.

Table 1. List of primers used for the RT-qPCR.

Oligonucleotides		
RT-qPCR		
CBP	Forward	ACCGGTGTAAGGAAAGGCTG
	Reverse	TCAGGTGTTGGGAAGATGGC
Survivin (BIRC5)	Forward	AGGACCACCGCATCTCTACAT
	Reverse	AAGTCTGGCTCGTTCTCAGTG
LGR5	Forward	TGCTCTTCACCAACTGCATC
	Reverse	CTCAGGCTCACCAGATCCTC
SOX9	Forward	GTACCCGCACTTGCACAAC
	Reverse	TCTCGCTCTCGTTCAGAAGTC
GAPDH	Forward	GAAATCCCATCACCAATCTTCCAGG
	Reverse	GCAATTGAGCCCCAGCCTTCTC
ChIP Promoter Target Primers		
Axin2	Forward	CTGGAGCCGGCTGCGCTTTGATAA
	Reverse	CGGCCCCGAAATCCATCGCTCTGA
c-MYC	Forward	AATGCCTTTGGGTGAGGGAC
	Reverse	TCCGTGCCTTTTTTTGGGG
CyclinD1	Forward	CGGGGCAGCAGAAGCGAGA
	Reverse	GTGAGTAGCAAAGAAACGTGG
LGR5	Forward	GCGATTTCTTTGAGGCTTTG
	Reverse	ATCCGAAAGATTGGCATCAC

Table 2. List of Antibodies.

List of Antibodies		
Reagent	**Source**	**Identifier**
Mouse anti-Actin Monoclonal Antibody	Millipore	MAB1501
Mouse monoclonal anti-GAPDH	Abcam	Caab8245; RRID: AB_2107448
Anti-Sam68 (rabbit antiserum)	Millipore	Cat#07-415; RRID: AB_310597
Mouse anti-CBP	BD Pharmingen	557021
Rabbit anti-E-cadherin	Cell Signalling	3195S
Mouse anti-ki67	BD Pharmingen	556003
Mouse anti-smooth muscle actin	R&D Systems	MAB1420
Goat anti-Mouse IgG (H+L) Highly Cross-Adsorbed Secondary Antibody, Alexa Fluor 488	Invitrogen	A-11029
Goat anti-Rabbit IgG (H+L) Highly Cross-Adsorbed Secondary Antibody, Alexa Fluor Plus 555	Invitrogen	A32732
Anti-Mouse secondary antibody	Promega	W402B
Anti-Rabbit IgG (H+L), HRP Conjugate	Bio-Rad	170-6515
IR-800CW 2DG Optical Probe	Li-COR	926-08946
Goat anti-Rabbit IgG (H+L) Highly Cross-Adsorbed Secondary Antibody, Alexa Fluor 488	Invitrogen	A11034
Anti-CBP Polyclonal	Invitrogen	PA5-27369
IgG Antibody	Santa Cruz	F1818
Foxa2 Polyclonal Antibody	R&D Systems	AF2400

Chapter 4

Results

4.1- ICG/CWP peptidomimetic compounds are direct interactors of Sam68

Considering the co-activator function of CBP in the context of cancer, efforts were deployed to develop small molecule inhibitors of its histone acetyltransferase activity. This includes the discovery and characterization of compounds selectively binding to CBP/p300 bromodomains, such as C646 and I-CBP112 (Figure 5A) (Conery et al., 2016b). ICG-001 and CWP232228 are two pioneer peptidomimetic compounds reported to block CBP co-activator functions in cancer, causing a downregulation of β-catenin-dependent transcription (Figure 5A) (Emami et al., 2004; Jang et al., 2015; Lee et al., 2019). Cell growth and differentiation experiments gave strikingly distinct results for side-by-side testing of CBP bromodomain inhibitors and ICG/CWP peptidomimetics in transformed human embryonic stem cells, which consists in a surrogate model of CSCs in culture (Benoit et al., 2017). While both type of compounds effectively reduced histone H3 acetylation (H3K14/18ac, **Figure 5B**), only peptidomimetic-based inhibition achieved substantial growth inhibition and differentiation onset (**Figure 5C, D**). Interestingly, the peptidomimetic CWP232228 did not reduce levels of activated β-catenin in t-hESCs upon 48-hour treatments (**Figure 5E**). This is consistent with previous observations where the levels of chromatin-bound β-catenin and TCF4 at canonical WNT target genes were not affected by CWP232228 (Benoit et al., 2017). As aforementioned, Sam68 was reported as a critical mediator

of CWP232228 antineoplastic response (Benoit et al., 2017). Despite several articles citing putative mechanism of action, it is still unclear whether ICG/CWP molecules directly interact with either CBP, β-catenin, and/or Sam68 in cancer cells. Therefore, we immobilized the active form of CWP232228 (CWP232904) on magnetic bead substrate to perform affinity pulldown experiments. CWP232904 is obtained from the hydrolysis of CWP232228 phosphate group by the action serum alkaline phosphatase (**Figure 5F**). CWP232904 was functionalized with a carboxylic group by succinic anhydride with the catalysis of DMAP. Then, carboxylic-CWP232904 was conjugated to amine-functionalized magnetic beads (**Figure 5G**). Affinity pull downs using CWP-conjugated beads and performed on human pluripotent whole cell lysates showed clear interaction between CWP232904 and Sam68 (**Figure 5G**, track 3). While only trace amounts of CBP were detected, no interaction were observed between immobilized CWP232904 and β-catenin, as well as with random test proteins such as MYB and GATA2 (**Figure 5G**, heatmap). Moreover, competition assays using excess of soluble CWP232904 or ICG-001 (100μM each) blocked the interaction between immobilized ligand and Sam68 (**Figure 5G**, tracks 4 and 5). It is noteworthy that CWP232228 treatments did not significantly impact Sam68 and CBP protein levels in t-hESCs (**Figure 5H**). Altogether, my results suggest that Sam68 is the primary target of ICG/CWP molecules in human neoplastic stem cells, and functional impacts observed upon treatments may be the consequence of downstream modulation of CBP/β-catenin interactions.

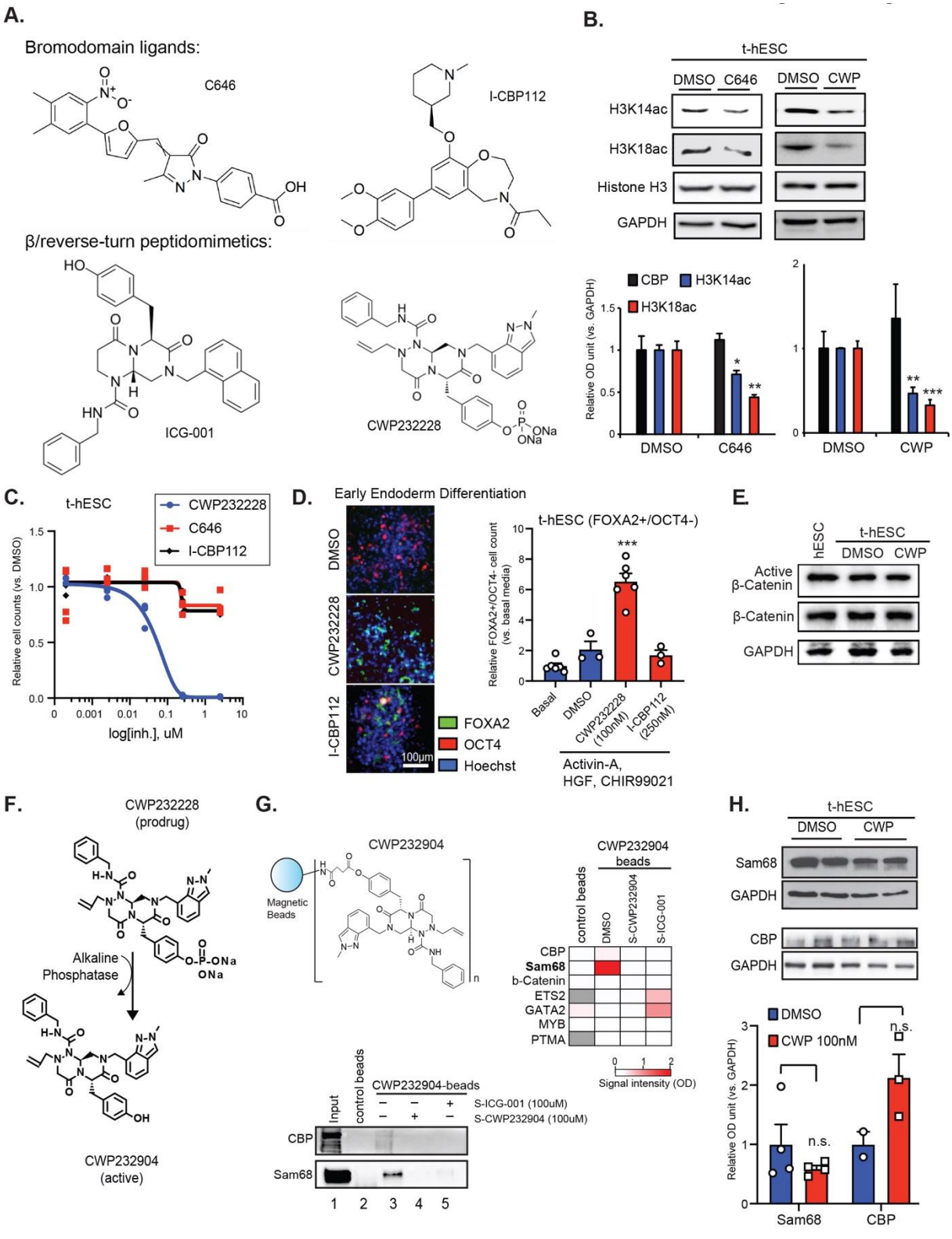

Figure 5. ICG/CWP peptidomimetic compounds are direct interactors of Sam68

A) Chemical structure of bromodomain ligands C646 and I-CBP112, as well as β-turn (ICG-001) and reverse-turn (CWP232228) peptidomimetics.

B) Western blot analysis of CBP-catalyzed H3K14ac and H3K18ac histone acetylation marks in C646 (250nM) and CWP232228 (100nM) t-hESCs vs. control DMSO. Total histone H3 and GAPDH were used as loading control. Relative OD signal quantification vs. H3 intensity are presented (H3K14ac: n=3, H3K18ac: n=6, *: p=0.0183, **: p≤0.0078, ***: p=0.00012).

C) Dose-response experiment assessing the impact of bromodomain ligand-based (C646 and I-CBP112), and peptidomimetic (CWP232228) inhibition of CBP on t-hESC growth (C646, I-CPB112: n=4; CWP232228: n=3).

D) Early endoderm differentiation assay performed on OCT4-GFP t-hESCs in the presence of CWP232228 (100nM, n=6) or I-CBP112 (250nM, n=3) vs. control DMSO (n=6) and basal culture media (n=3). Bar graph represents relative counts of FOXA2-positive (early endoderm marker) / OCT4-negative cells in DMSO, CWP232228, and I-CBP-treated t-hESCs vs. basal culture media (One-way ANOVA, ***: p<0.0001). Scale bar: 100um

E) Western blot analysis of active β-catenin and total β-catenin levels in H9 normal human ES (hESC) and t-hESCs treated with CWP232228 (100nM, 48h) vs. control DMSO. GAPDH was used as loading control.

F) Pro-drug CWP232228 is converted into its active form CWP232904 via hydrolysis of the phosphate group by serum alkaline phosphatase.

G) Affinity pulldown experiments using CWP232904-conjugated magnetic beads performed on whole hESC lysates. Physical interaction between CBP, Sam68, β-catenin, and other putative CBP

interactors MYB, and GATA2 and immobilized CWP232904 was assessed by western blot. OD quantification is presented as a heat map. Excess of soluble compounds (CWP and ICG001, 100uM) were used to compete with immobilized CWP232904. Whole cell lysate was used as input and amine-functionalized beads were used as negative control (n=2).

H) Western blot analysis of Sam68 and CBP levels in CWP232228-treated (100nM, 48h) t-hESCs vs. control DMSO. GAPDH were used as loading control. Relative OD signal quantification vs. GAPDH intensity is presented in the bar graph (Sam68: n=4, CBP: n=3, n.s.: not significant).

4.2- Sam68-SRC interaction is a “druggable” target in cancer

Direct binding of small molecule to Sam68 has been previously reported as a way to inhibit SH3-dependent interaction with SRC (Oneyama et al., 2002). Specifically, the small molecule UCS15A was shown to disrupt Sam68 interactions with different SH3 motif-containing proteins in human colorectal cancer cells HCT116, including SRC, GRB2, and PLCγ (Oneyama et al., 2002). Extensive molecular investigations concluded that UCS15A blocks Sam68 protein-protein interactions by directly targeting its P4 and P5 proline-rich domains (**Figure 6A**) (Oneyama et al., 2002). I used TASSER-VMT algorithm to build a structural model of a fragment of Sam68 including amino acids 275 to 374 (Sam68 275-374) (Zhou and Skolnick, 2012). This fragment includes proline-rich domains P3 to P5 involved in SH3-mediated protein-protein interactions (**Figure 6A**). Next, I used the platform LigPlot+ to predict a 2D ligand-protein interaction diagram of UCS15A within Sam68 275-374 peptide (**Figure 6B**) (Laskowski and Swindells, 2011). I conducted a similar predictive analysis using the first-generation β-turn peptidomimetic compound ICG-001, and observed a binding pocket involving several residues in common with Sam68-UCS15A interaction (**Figure 6B**). Although, ICG-001 presented selective growth inhibition toward human colorectal cancer cells vs. normal intestinal progenitors, its potency was deemed to be low, with a calculated EC50 above 10μM in HT29 cell lines (**Figure 6C**). CWP232228 also demonstrated selective growth inhibition in HT29 cells, but its potency was significantly higher with a calculated EC50 of 0.65μM (**Figure 6C**). Still, both peptidomimetic compounds presented safety issues in preclinical and clinical phases, advocating the need to develop novel peptidomimetic inhibitors of Sam68 protein-protein interactions with higher potency (Cortes et al., 2015; Ko et al., 2016).

The main structural variations between ICG-001 and active CWP232904 are found at position “A” and “B”, as indicated in **Figure 6D**. Thus, I initiated an *in silico* structural activity relationship endeavour, predicting docking affinity of a library of 125 ICG/CWP peptidomimetic analogs for the Sam68 275-374 peptide. SMILE code for each ICG/CWP analogs were generated based on molecular structures from the patent US8101751B2. I used the software AutoDock Vina to obtain predicted change in free energy (ΔG) for each ligand-protein complex formation (**Figure 6E**) (Gaillard, 2018; Trott and Olson, 2010). All analogs presenting a standard deviation wider than 0.1 were excluded and individual constants of equilibrium (Keq) were calculated from ΔG values to establish a compound ranking based on affinity for Sam68 proline-rich domains (**Figure 6F**) (Ref for Keq calculation). An arbitrary cut-off was set to select putative compounds showing >10-fold higher affinity for Sam68 275-374 vs. UCS15A (**Figure 6G**). Despite poor potency in cellular systems, ICG-001 scored among the strongest binders of Sam68 275-374 (**Figure 6F, G**). Such an exercise highlighted a putative structure (YB-0159) closely related to CWP232904, presenting a 1H-indazole function in position “B”, instead of 2-methyl-2H-indazole, and showing a predicted binding affinity ~20-fold and ~50-fold superior to CWP232904 and UCS15A, respectively, for Sam68 P3-P5 proline-rich domains (**Figure 6H**). The putative prodrug structure was named YB-0158 and included a hydrolysable phosphate moiety similar to CWP232228 (**Figure 6H**).

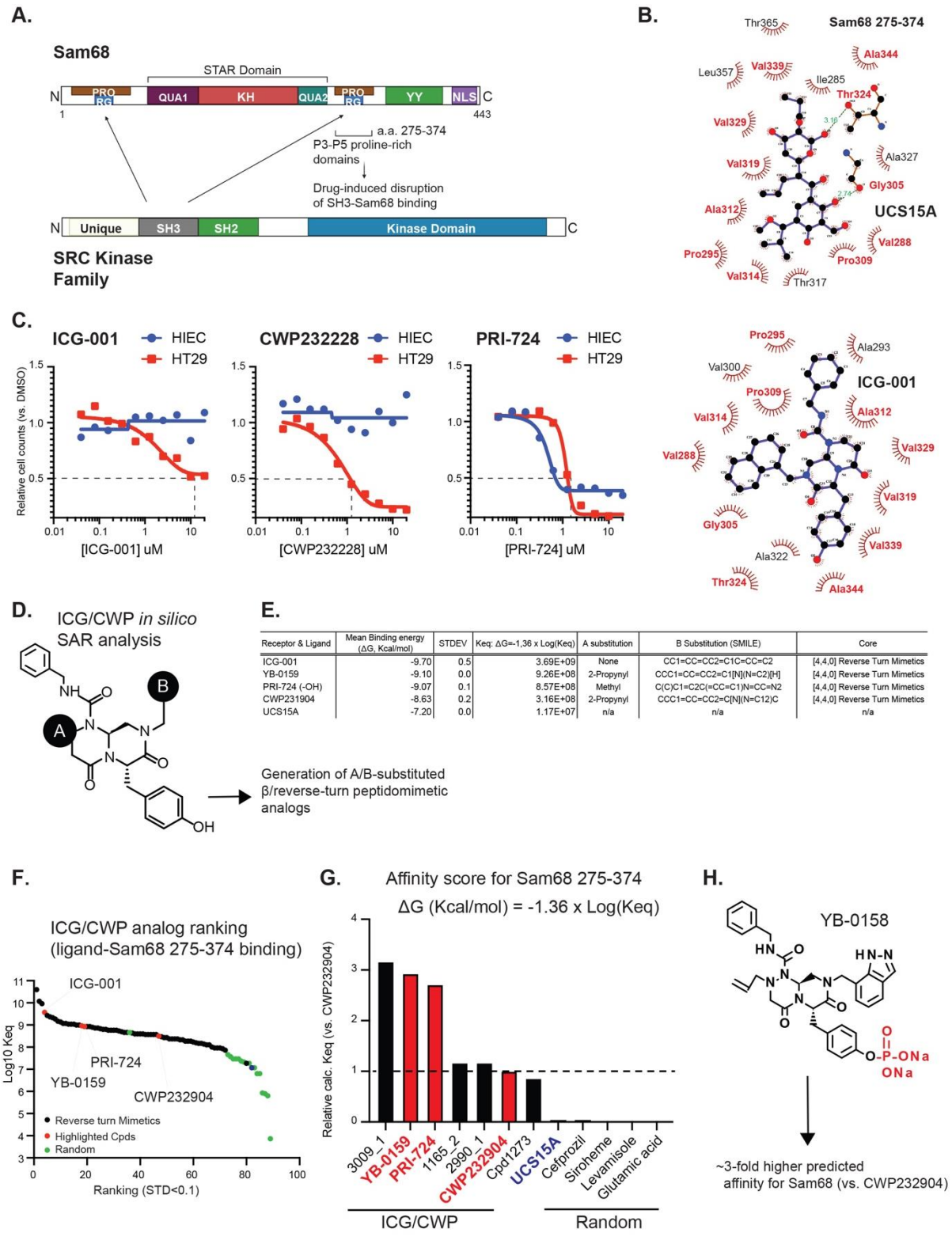

Receptor & Ligand	Mean Binding energy (ΔG, Kcal/mol)	STDEV	Keq: ΔG=-1,36 x Log(Keq)	A substitution	B Substitution (SMILE)	Core
ICG-001	-9.70	0.5	3.69E+09	None	CC1=CC=CC2=C1C=CC=C2	[4,4,0] Reverse Turn Mimetics
YB-0159	-9.10	0.0	9.26E+08	2-Propynyl	CCC1=CC=CC2=C1[N](N=C2)[H]	[4,4,0] Reverse Turn Mimetics
PRI-724 (-OH)	-9.07	0.1	8.57E+08	Methyl	C(C)C1=C2C(=CC=C1)N=CC=N2	[4,4,0] Reverse Turn Mimetics
CWP231904	-8.63	0.2	3.16E+08	2-Propynyl	CCC1=CC=CC2=C[N](N=C12)C	[4,4,0] Reverse Turn Mimetics
UCS15A	-7.20	0.0	1.17E+07	n/a	n/a	n/a

Figure 6. YB-0158 is a novel peptidomimetic compound predicted to bind Sam68

A) Sam68 is interacting with SH3 domain in SRC kinase family via proline-rich motifs located in N-terminal P1-P2 and between residues 275-374 (P3, P4, P5). Small molecule UCS15A is known to disrupt SH3-mediated interaction of SRC with Sam68 P3-5 domains.

B) 2D representation of UCS15A and the peptidomimetic ICG-001 *in silico* predicted binding pocket in Sam68 275-374 peptide. Common residues involved in both small molecule binding pocket are highlighted in red. Predicted hydrogen bonds are represented by dashed lines.

C) Dose-response curves assessing selective toxicity of peptidomimetics ICG-001, CWP232228 and PRI-724 in HT29 human colorectal cancer cell line vs. normal intestinal progenitor cells HIEC ($n \geq 4$, 48h treatments).

D) Structural differences between active ICG/CWP molecules consist in distinct substituents at positions defined as “A” and “B”.

E) Curated table of different ICG/CWP analogs and their respective *in silico* predicted binding energy for Sam68 275-374 interaction (Exhaustiveness (“E”) set to 50).

F) Compound ranking based on predicted Keq for each ICG/CWP analog (black dots). Only molecules presenting a standard deviation below 0.1 for a minimum of 3 analysis runs, with an exhaustiveness (E) level of “8” were plotted. Dots corresponding to ICG-001, CWP232228, PRI-724, and YB-0159 were highlighted in red. Random structure ranking is represented by green dots.

G) Bar graph representing relative Keq values (in silico prediction) for select ICG/CWP analogs. CWP232904 Keq was set as the reference.

H) Structure of YB-0158, a phosphate-stabilized prodrug of YB-0159.

Next, 3D and 2D structural models of YB-0159 interaction with Sam68 were generated using Chimera and LigPlot+ algorithms, respectively (**Figure 7A-C**). Comparison of predicted binding pockets of YB-0159 and CWP232904 within Sam68 275-374 region revealed the involvement of several amino acids in common with ICG-001 interaction site (highlighted in red: **Figure 7C**). Interestingly, YB-0159 2D model displays two hydrogen bonds (3.04Å and 2.80Å) between glycine 305 and nitrogen N7 and N6 in YB-0159, which is absent from CWP232904 model, potentially due to the presence of the methyl group (C33) on the indazole function (**Figure 7C**). This could explain the higher Keq value obtained for YB-0159 in docking analysis versus CWP232904. Thus, we generated 3 in silico mutants of Sam68 275-374, in which glycine 305 was substituted by either alanine (G305A), asparagine (G305N), or serine (G305S) (**Figure 7D**). With the help of colleagues, I repeated docking analysis for both, YB-0159 and CWP232904 but using mutant peptides (E=50). Comparison of calculated Keq obtained for each mutant vs. wt Sam68 fragment revealed that the absence of a glycine in position 305 significantly reduces binding affinity with YB-0159 (**Figure 7E**). Remarkably, G305 substitution had no significant impact of CWP232904 predicted binding energy (Figure 7E). It will be interesting, in the future, to test the impact of Sam68 G305 substitution in functional experiments, to determine its relevance to YB-0159 anticancer response in human systems.

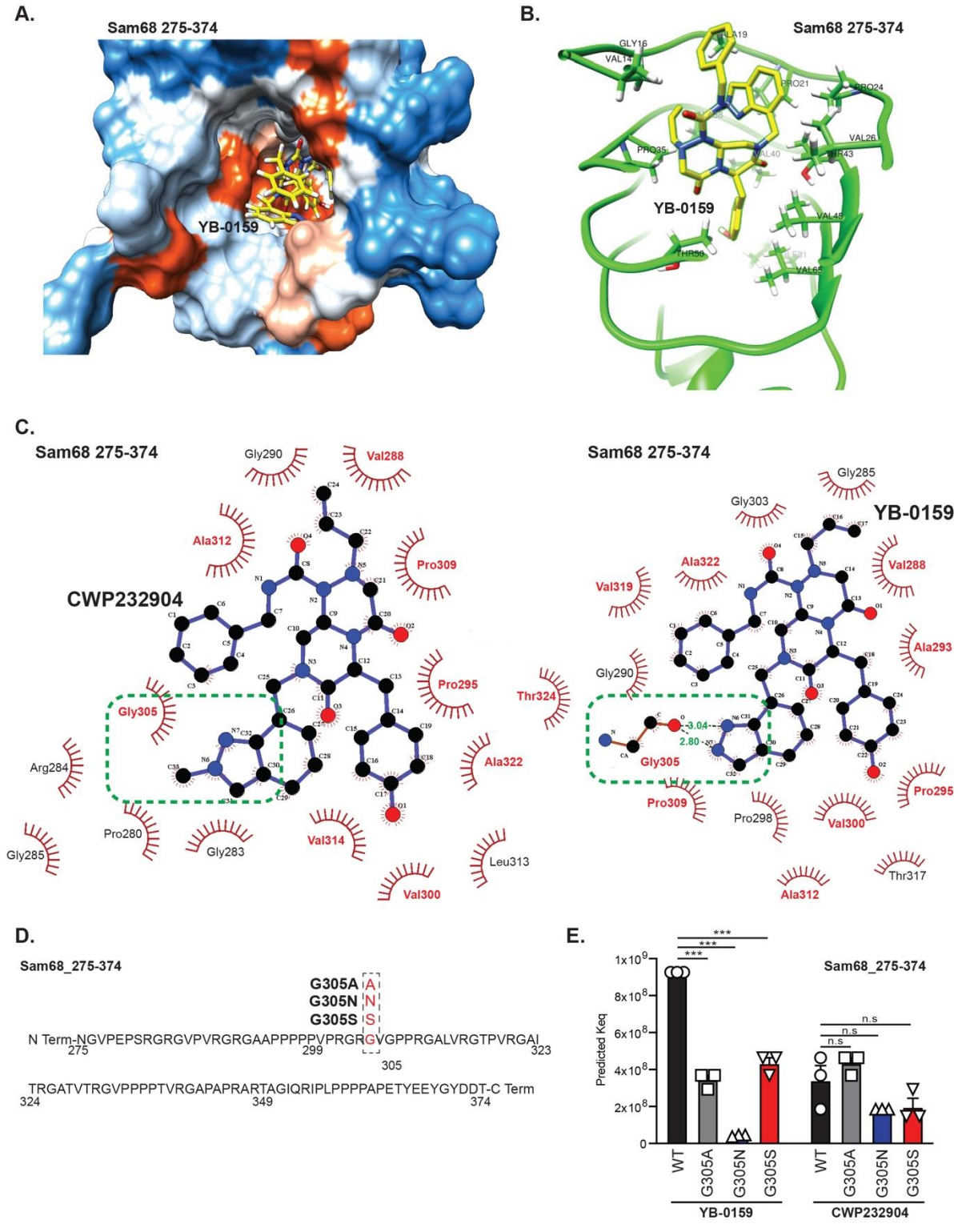

Figure 7. In Silico identification of key molecular determinants of Sam68-YB-0159 interactions

A) Electrostatic surface representation of Sam68 275-374 structure interacting with YB-0159 ligand.

B) Ribbon representation of Sam68 275-374 structure interacting with YB-0159 ligand.

C) 2D diagrams of CWP232904 and YB-0159 binding pockets within Sam68 275-374 fragment. Residues also implicated in ICG-001 binding are highlighted in red. The green dashed region emphasizes the site of putative H-bonds between YB-0159 and Sam68 G305.

D) Amino acid sequences used to generate 3D structure of 3 single-residue substitution mutants of Sam68 275-374 peptide (G305A, G305N, G305S).

E) Calculated constants of equilibrium (Keq) upon docking analysis of Sam68 275-374 wt and mutants, with YB-0159 and CWP232904. E50 analyses of each complex were performed 3 times (***: $p<0.0001$).

4.3- YB-0158 is a highly potent analog of CWP232228, disrupting Sam68-SRC interaction and reducing CBP chromatin recruitment

Upon identification of YB-0158 as a putative high-affinity ligand of Sam68, potentially disrupting Sam68-SRC interaction, we got the small molecule synthesized by Haoyuan Chemexpress (China) and tested its potency in biological assays. Dose-response experiments confirmed that YB-0158 displays ~10-fold and ~5-fold superior potency vs. CWP232228 to inhibit cell growth in t-hESCs and human colorectal cancer HT29 cells, respectively (**Figure 8A, B**). As previously demonstrated for its closely-related analog CWP232228, YB-0158 also induced a loss of pluripotency in t-hESC, characterized by a decrease in OCT4 expression, which consists in a critical factor for pluripotency maintenance (**Figure 8C**) (Benoit et al., 2017). Based on previous literature, this supports the potential of YB-0158 to alter key neoplastic stem cell functions, such as pluripotent-like transcriptional signatures (Ben-Porath et al., 2008; Bergin et al., 2020; Sachlos et al., 2012). However, no differences were observed between the two small molecule analogs regarding their potency to induce such a change in OCT4 expression. Using co-immunoprecipitation assay, I demonstrated that both, YB-0158 and CWP232228 have the capacity to disrupt Sam68-SRC interactions in human colorectal cancer, when used at calculated EC50 concentrations (**Figure 8D**). Moreover, western blot analysis revealed no changes of SRC tyrosine 416 phosphorylation status, supporting previous findings indicating that small molecule-based disruption of Sam68-SH3 interactions has no impact on SRC autophosphorylation kinase activity (**Figure 8E**) (Sharma et al., 2001). Altogether, these observations support our *in silico* modelling approach to identify small molecule structures potentially mimicking UCS15A effect on Sam68 P3-P5 proline-rich domain interaction with SRC SH3 motif. Additional experiments validating the impact of YB-0158,

and other ICG/CWP analogs on molecular events downstream of Sam68/SRC complexes will be necessary to strengthen my observations.

Previous studies in human renal cancer demonstrated that high Sam68 cytoplasmic localization was significantly associated with poor survival (Zhang et al., 2009). Moreover, ICG-001 and CWP232228 treatments caused significant accumulation of Sam68 in the nucleus of t-hESCs (Benoit et al., 2017). Thus, I used immunofluorescence of Sam68, followed by high-content imaging to quantify nuclear Sam68 signal in t-hESC treated with increasing doses of YB-0158 and CWP232228 (0 to 125nM, 48h) (**Figure 8F**). I observed that lower doses of YB-0158 were necessary to induce significant Sam68 accumulation (≥16nM) compared to CWP232228 (≥125nM) (**Figure 8F**). Moreover, YB-0158 was shown to also cause significant Sam68 nuclear accumulation in HT29 colorectal cancer cells, but at a higher dose range than in t-hESC (**Figure 8G**). Hence, Sam68 nuclear shuttling upon YB-0158 or CWP232228 treatments could be a consequence of cytoplasmic SRC-Sam68 complex disruption. Increased levels of nuclear Sam68 in human neoplastic stem cells was previously shown to increase the frequency of interactions with the transcriptional co-activator CBP (Benoit et al., 2017; Hong et al., 2002b). As a result, CBP is sequestered from the chromatin, leading to downregulation of WNT/β-catenin target gene expression (Benoit et al., 2017). Akin to CWP232228, chromatin immunoprecipitation (ChIP) assays revealed that YB-0158 treatments decreased CBP recruitment to the promoter of WNT/β-catenin target genes LGR5, AXIN2, CCND1, and c-MYC in HT29 cells, compared to DMSO control (**Figure 8H**). As for growth inhibition experiments (**Figure 8A, B**), doses of YB-0158 sufficient to induce Sam68-SRC disruption, Sam68 nuclear accumulation, and inhibition of CBP chromatin recruitment (**Figure 8D, F-H**) were ~5 to 10-fold lower versus CWP232228, depending on the cell

model tested. Taken together, my observations support the relevance of Sam68 as a key mediator of YB-0158 antineoplastic response.

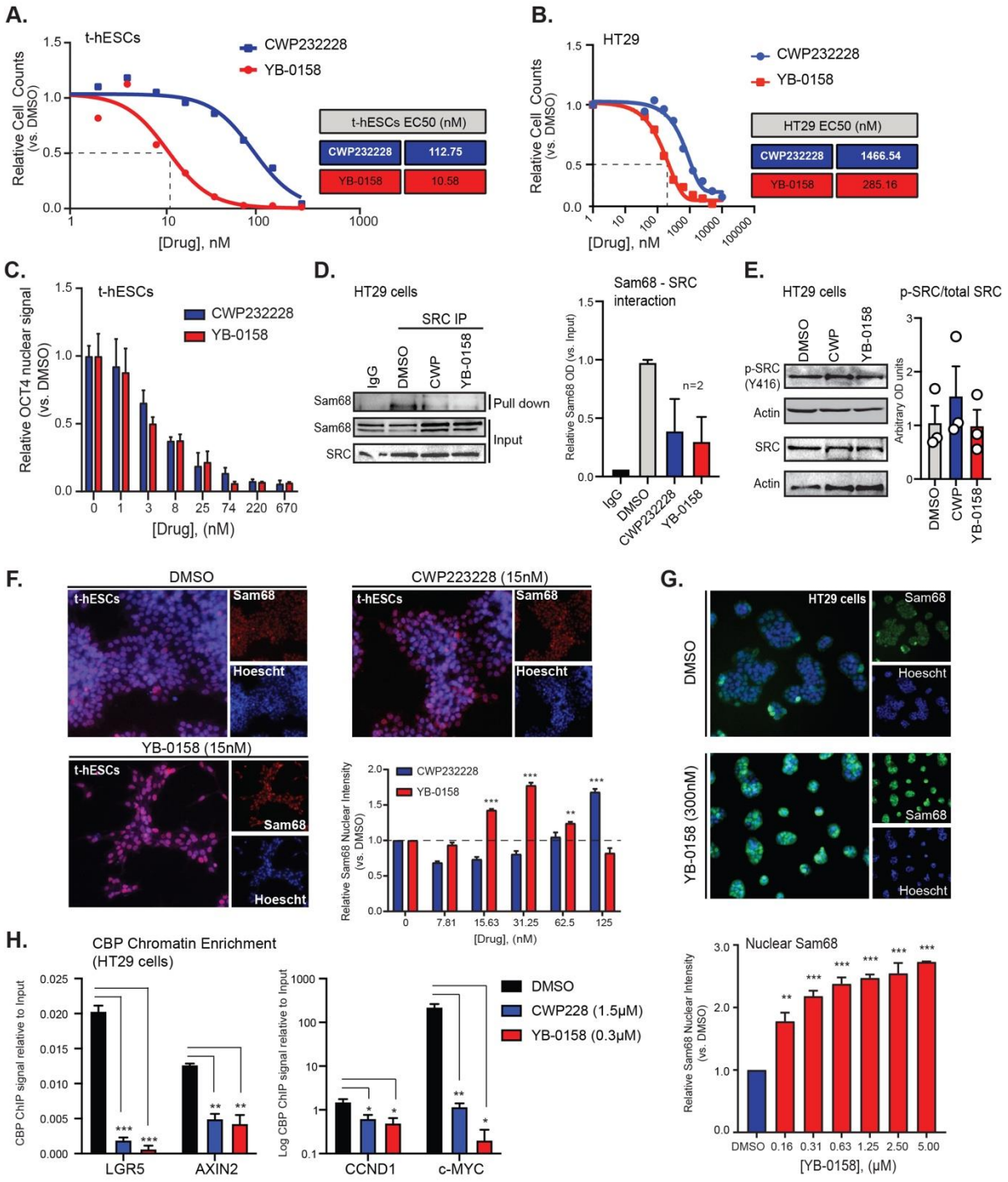

Figure 8. YB-0158 impacts SRC activation, Sam68 distribution, and CBP chromatin recruitment in human colorectal cancer cells

A) Dose-response experiment assessing growth inhibition caused by peptidomimetics analogs CWP232228 and YB-0158 in t-hESCs (n=3, 48h treatments). Calculated EC50 for each small molecule is presented in inset table.

B) Dose-response experiment assessing growth inhibition caused by peptidomimetics analogs CWP232228 and YB-0158 in HT29 colorectal cancer cells (n=2, 48h treatments). Calculated EC50 for each small molecule is presented in inset table.

C) High-content imaging-based quantification of nuclear OCT4 levels in t-hESCs treated with increasing doses of CWP232228 and YB-0158 (n=3, 48h).

D) Co-immunoprecipitation (IP) assessing changes in interaction levels between SRC and Sam68 in response to CWP232228 (1.5µM) and YB-0158 (0.3µM) in HT29 cells (48h). Both small molecules were used at calculated EC50 doses, as reported in panel B. Mouse IgGs were used as negative control for pull down.

E) Western analysis of SRC phosphorylation (Y416) levels in HT29 cells upon CWP232228 (1.5µM) and YB-0158 (0.3µM) treatment vs. vehicle control (48h, n=3).

F) Sam68 immunostaining in DMSO, CWP232228, and YB-0158-treated t-hESCs (48h, n=9). Quantification of nuclear Sam68 nuclear was performed by high-content imaging and presented as relative levels vs. DMSO (**: $p<0.01$, ***: $p<0.0001$).

G) Sam68 immunostaining in DMSO and YB-0158-treated HT29 cells (48h, n=6). Quantification of nuclear Sam68 nuclear was performed by high-content imaging and presented as relative levels vs. DMSO (**: $p=0.008$, ***: $p<0.0001$).

H) Chromatin immunoprecipitation (ChIP) analysis of CBP occupancy at canonical Wnt target promoters (LGR5, AXIN2, CCND1 and c-Myc) following CWP232228 (1.5µM) and YB-0158 (0.3µM) treatments vs. DMSO in HT29 cells (48h). Data were presented as ChIP signal relative to input. (n=3, *: $p \leq 0.0324$, **: $p \leq 0.0027$, ***: $p < 0.0001$).

4.4- Sam68 expression mediates cancer-selective response to YB-0158 in human colorectal cancer cells

An key aspect of the development of novel anticancer therapeutics resides in the degree of toxicity observed in healthy tissues versus tumor cells. As highlighted in **Figure 6C**, ICG-001 and CWP232228 display lower EC50 values for cell growth inhibition in colorectal cancer cells compared to normal human intestinal progenitors. To gain further insights into such a cancer-selective toxicity, I profiled transcript expression of key factors involved in the molecular mechanism of action of ICG/CWP molecules in colon (COAD) and rectal (READ) adenocarcinomas isolated from human patients. Such factors include canonical WNT transactivators CBP, p300, and β-catenin, as well as Sam68 and SRC. It is noteworthy that Sam68 expression was significantly more abundant in colon and rectal tumors compared with healthy tissues (**Figure 9A**). Higher expression of canonical WNT target genes LGR5 and Survivin in tumors vs. normal tissues confirmed the oncogenic hyperactivation of such a key signaling pathway in cancer (**Figure 9A**). Similar observations were made in various human and murine colorectal models, where Sam68 protein levels were elevated in transformed lines (SW480, HCT116, HT29, MC38) while only traces of expression was detected in normal human intestinal progenitor cells HIEC (**Figure 9B**). Moreover, Sam68 expression was higher in colorectal cancer patient-derived spheroids vs. bulk 3D colorectal tumor organoids resulting from single-cell seeding (de Sousa e Melo et al., 2017; O'Brien et al., 2007) (**Figure 9B**). By opposition to CSC-enriched spheroids, 3D organoids were described as mini tumors maintaining primary patient tumor heterogeneity (Lima-Fernandes et al., 2019). Accordingly, cell growth experiments confirmed that YB-0158 displays a lower EC50 in colorectal models expressing high levels of Sam68, compared to normal HIEC cells (**Figure 9C**).

This further supports the cancer-selective toxicity of ICG/CWP molecules over healthy tissues (**Figure 6C**) (Benoit et al., 2017).

To validate the essential participation of Sam68 in YB-0158 anticancer response, I performed shRNA-based knockdown experiments of putative ICG/CWP targets, followed by growth assessment in drug-treated HT29 cells. Five independent shRNA hairpins targeting Sam68 or CBP mRNA, I generated stable Sam68 (shSam68) and CBP (shCBP) knockdown, as well as scramble shRNA-expressing (shCTRL) HT29 populations. Western blot analysis was used to determine which shRNAs yield the best knockdown efficiency for Sam68 and CBP (**Figure 9D, E**). Next, I performed dose-response growth experiments using Sam68 knockdown and shCTRL HT29 cells exposed to increasing concentrations of YB-0158. Interestingly, Sam68 knockdown cells displayed significantly higher growth rate when treated with YB-0158 vs. shCTRL cells (**Figure 9D,** 0.08 to 0.63μM, red dashed box). Specifically, I observed a ~2-fold increase of calculated EC50 value (0.625μM) in shSam68 HT29 cells compared to controls (290μM) (**Figure 9D**). Such a phenomenon was not observed in CBP knockdown HT29 cells vs. control shRNA population (**Figure 9E**). Importantly, I observed no effects of Sam68 knockdown on HT29 basal growth rate compared to shCTRL. Taken together, these observations demonstrated that Sam68 expression plays a central role in YB-0158 mechanism of action, and further supports its direct interaction with Sam68, as demonstrated by affinity pull down assays and in silico modelling.

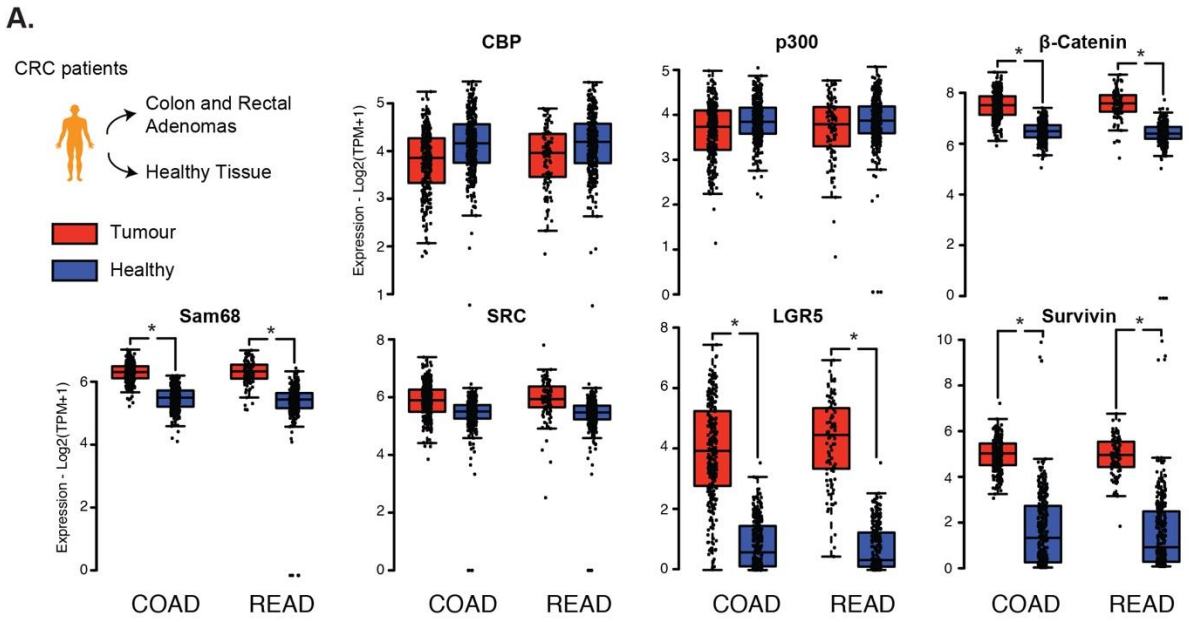
A.
CRC patients
Colon and Rectal Adenomas
Healthy Tissue
Tumour
Healthy
CBP
p300
β-Catenin
Sam68
SRC
LGR5
Survivin
Expression - Log2(TPM+1)
COAD
READ

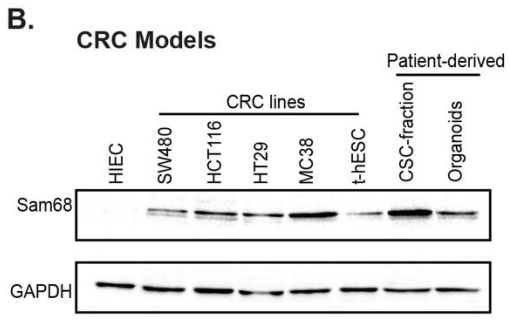
B.
CRC Models
Patient-derived
CRC lines
HIEC
SW480
HCT116
HT29
MC38
t-hESC
CSC-fraction
Organoids
Sam68
GAPDH

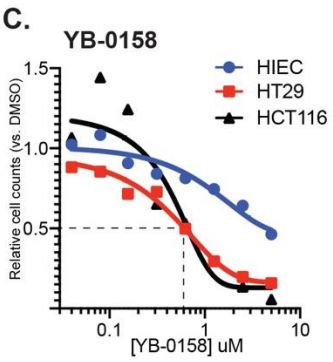
C.
YB-0158
HIEC
HT29
HCT116
Relative cell counts (vs. DMSO)
[YB-0158] uM

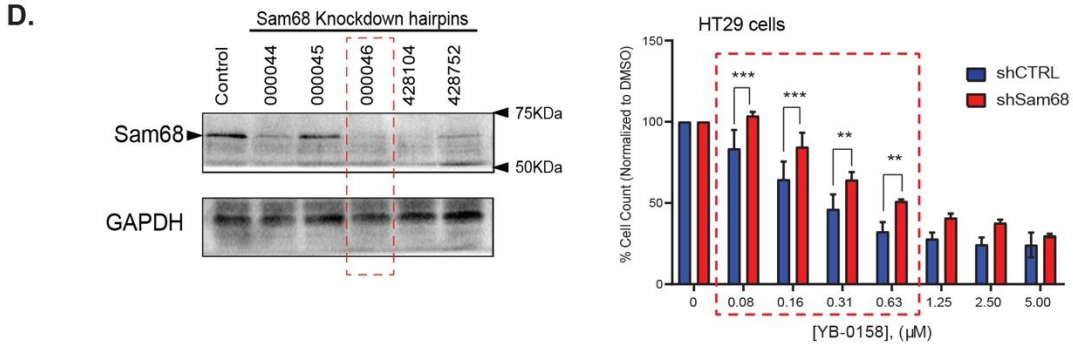
D.
Sam68 Knockdown hairpins
Control
000044
000045
000046
428104
428752
Sam68
GAPDH
75KDa
50KDa
HT29 cells
shCTRL
shSam68
% Cell Count (Normalized to DMSO)
[YB-0158], (μM)

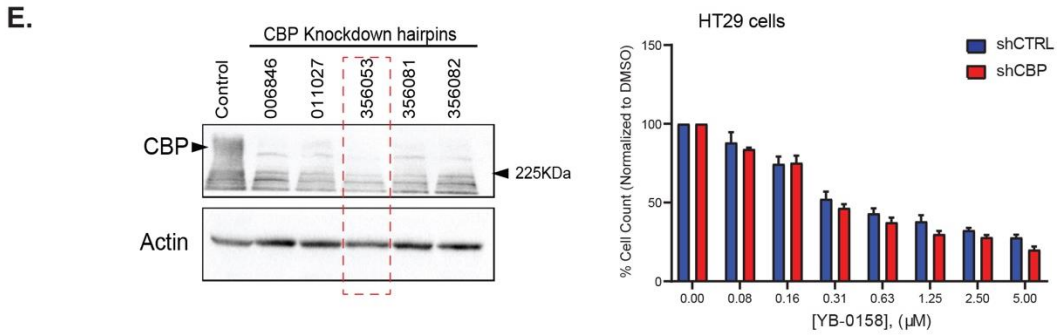
E.
CBP Knockdown hairpins
Control
006846
011027
356053
356081
356082
CBP
Actin
225KDa
HT29 cells
shCTRL
shCBP
% Cell Count (Normalized to DMSO)
[YB-0158], (μM)

Figure 9. Sam68 expression mediates cancer-selective response to YB-0158

A) Box plots of key canonical WNT transcriptional activators (CBP, p300, β-catenin), Sam68/SRC axis, and ICG/CWP-responsive genes (LGR5, Survivin) profiled by RNA-seq in human colon and rectal adenocarcinoma (TCGA COAD, n=275 vs. normal, n=41, TCGA READ, n=92 vs. normal, n=318). Values are expressed as TPM (***: $p<0.0001$, Log2FC cutoff: >0.5, p-value cutoff: 0.0001).

B) Western blot analysis of Sam68 levels in normal human intestinal progenitor cells HIEC, human colorectal cancer SW480, HT29, and HCT116 lines, mouse colon adenocarcinoma MC38 cells, t-hESCs, as well as patient-derived CSC-enriched spheroids and 3D organoids from colorectal tumor samples ($n\geq3$). GAPDH was used as loading control. Relative OD signal quantification for Sam68 vs. GAPDH intensity is presented.

C) Dose-response experiment monitoring growth of normal intestinal cells HIEC, as well as HT29 and HCT116 colorectal cancer lines treated with YB-0158 ($n\geq3$, 48h).

D) Growth assessment of Sam68 knockdown and control shRNA (shCTRL) HT29 cells, treated with increasing doses of YB-0158 (0 to 5μM, 48h). Efficiency of 5 independent Sam68-targeting shRNAs was tested by western blot. Dose-response experiments were conducted using hairpin #000046 (n=3, **: $p<0.01$, ***: $p\leq0.006$).

E) Growth assessment of CBP knockdown and control shRNA (shCTRL) HT29 cells, treated with increasing doses of YB-0158 (0 to 5μM, 48h). Efficiency of 5 independent CBP-targeting shRNAs was tested by western blot. Dose-response experiments were conducted using hairpin #356053 (n=2).

4.5- YB-0158 alters proliferation, apoptosis, and regulation of WNT/β-catenin targets in human colorectal cancer cells

Previously characterized ICG/CWP analogs (ICG-001, PRI-724, CWP232228) were shown to impact cancer cell functions such as proliferation, differentiation, and apoptosis via modulation of canonical WNT pathway (Benoit et al., 2017; Emami et al., 2004; Gabata et al., 2020). As mentioned in **Section 4.3**, YB-0158 treatments in human colorectal cancer cells cause an inhibition of CBP recruitment at the promoter of key WNT/β-catenin target genes (**Figure 8H**). Thus, I performed EdU incorporation assays, as well as live active caspase-3/7 staining to test whether YB-0158 is impacting key functions of colorectal cancer cells, such as proliferation and apoptosis, respectively. EdU incorporation assays, marking cells in S-phase of the cell cycle indicated that YB-0158 significantly impaired proliferation in HT29 cells compared to control DMSO (**Figure 10A**). Moreover, I observed that YB-0158 has a stronger inhibitory impact on HT29 proliferation than CWP232228, when both were tested at 200 and 500nM (**Figure 10A**). Active caspase-3/7 detection in HT29 cells revealed that YB-0158 is significantly increasing apoptosis at 500nM vs. DMSO control, while 200nM treatments were insufficient to affect cell survival rates (**Figure 10B**). My data indicate that YB-0158, when used at calculated EC50 (~290nM) is blocking colorectal cancer cell growth mainly via inhibiting proliferation rather than promoting apoptosis.

ICG/CWP molecules are known as inhibitors of WNT/β-catenin pathway, causing dissociation of CBP from chromatin-bound TCF/β-catenin complexes, consequently leading to a downregulation of target gene expression (Benoit et al., 2017; Kahn, 2014). Thus, using quantitative PCR (qPCR) analysis I validated that YB-0158 (200nM) is downregulating the expression of WNT/β-catenin

target genes SOX9, LGR5, and Survivin in HT29 cells compared to DMSO control (**Figure 10C**). Importantly, LGR5 is described in the literature as an important marker of colorectal cancer stem cells (CCSCs) (de Sousa e Melo et al., 2017). YB-0158-induced downregulation of LGR5 supports previous findings that ICG/CWP molecules have the potential to block CSC activity. Whole transcriptome profiling of control and YB-0158-treated colorectal cancer cells is currently underway to determine the broader impact of this new small molecule on the regulation of different gene networks. For instance, it will be interesting to determine whether YB-0158 can affect cell differentiation state of HT29 cells, which basically maintain an undifferentiated phenotype in standard culture conditions. Moreover, we will perform side-by-side comparisons of transcriptional modulation exerted by YB-0158 in human colorectal cancer cells with the effects of CWP232228 on global gene regulation. This will provide us with important insights into the mechanism of action of YB-0158 and closely related ICG/CWP analogs in cancer, which still needs to be fully understood.

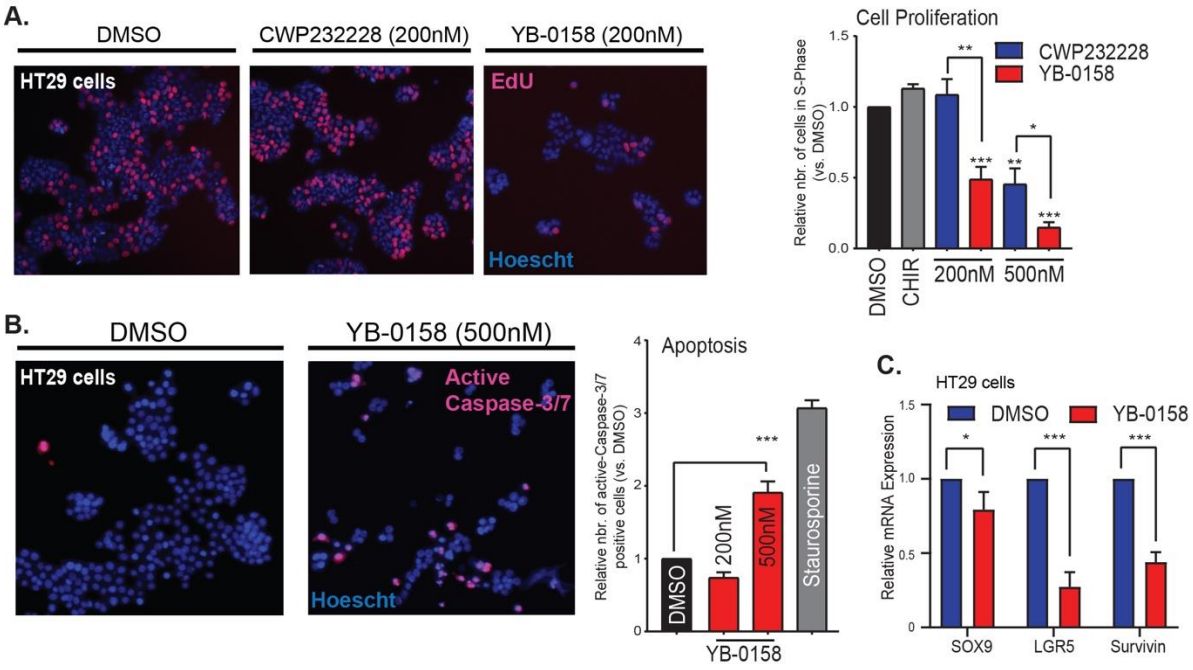

Figure 10. YB-0158 impacts proliferation, apoptosis, and expression of WNT/β-catenin target genes in human colorectal cancer cells

A) EdU incorporation assay labeling cells in S-phase indicates proliferation rates in CWP232228 and YB-0158-treated (48h) HT29 cells vs. DMSO control. CHIR99021 was used as a canonical WNT activation control (3μM). Relative number of EdU-positive cells was determined by high-content imaging (n≥3, *: p=0.0257, **: p≤0.0017, ***: p<0.0001).

B) *In situ* fluorescent staining of activated caspase-3/7 in YB-0158 treated HT29 cells (48h, 200nM and 500nM) compared to DMSO control. Staurosporine (6h, 1μM) was used as a positive control for apoptosis induction (n=3, ***: p<0.0001).

C) Quantitative PCR analysis of the expression of WNT/β-catenin target genes (SOX9, LGR5, Survivin) in YB-0158 (200uM) and DMSO-treated HT29 cells (48h, n=3, *: p=0.0388, ***: p≤0.0002).

4.6- YB-0158 blocks tumor-initiating capacity in primary colorectal cancer patient samples

To further explore the functional role of YB-0158 in CCSC populations present in patient-derived tumor samples, I used a serial organoid formation assay and tested the potential of YB-0158 to affect the tumor-initiating capacity of primary CCSCs. The course of this organoid formation assay is illustrated in **Figure.11A**. One of the key characteristics of CSCs resides in their capacity to initiate tumor formation (Kreso and Dick, 2014) and Patient-Derived Organoids (PDO) enable the study of human solid tumors initiated from a single stem cell in a 3D system (Tuveson and Clevers, 2019). PDOs recapitulate functional and morphological characteristics of their primary tissue of origin, and can be used to predict drug response in a pre-clinical or clinical in vivo setting (Tuveson and Clevers, 2019). PDO formation assays using primary human colon cancer specimens was shown to be a powerful method to test the impact of drugs on tumor-initiation activity (Crespo et al., 2017; Lima-Fernandes et al., 2019). Briefly, surgically-resected pieces of colon tumors from consenting patients were minced and enzymatically dissociated in Collagenase A. Once put in ultra-low adhesion culture conditions, in a serum-free media supplemented with bFGF, EGF, and a cocktail of soluble factors (N2 and B27 supplements), CSCs were enriched from bulk cell suspensions via formation of spheroids. CSC enrichment from spheroid cultures was previously confirmed in our lab based on flow cytometry profiling of key surface markers (CD133+/CD44+), as well as high expression of other key CCSC biomarkers such as LGR5 and G9a vs. bulk tumor sample (Bergin et al., 2020). Patient specimens used in the context of my work were obtained from Catherine O'Brien (U of Toronto) and via collaboration with Dr. Rebecca Auer (Ottawa Hospital Research Institute (OHRI). The clinical information about the three patient samples used

in our study is presented in **Figure 11B**. To establish tumor organoid cultures, CSC-enriched spheroids were dissociated and passed through a 70μm strainer to eliminate non-single-cell aggregates. Patient-specific cell suspensions were mixed with Matrigel in spheroid culture media. Cell-Matrigel mixtures were immediately plated as 300 μl domes in 6-well plates. By opposition to spheroids, 3D organoids were described as mini tumors maintaining primary patient tumor heterogeneity (Lima-Fernandes et al., 2019). A first series of organoid formation was conducted on 3 patient-derived samples, using working doses of the YB-0158 ranging from 0.125 to 2μM (vs. DMSO control) added to each organoid-containing dome and incubated for 7 days. Drug treatments were followed by a 7-day drug-free incubation (**Figure.11A**). At day-14, organoids were imaged and PDO frequency was determined for each well. YB-0158 treatments in a primary series of patient-derived 3D organoids resulted in a significant decrease of frequency compared to vehicle-treated groups (**Figure.11C, E**). Residual primary organoids were dissociated and re-seeded in a secondary series. Importantly, no further drug treatments were performed on this secondary series of PDOs, enabling bona fide assessment of persisting tumor-initiating cell populations in samples previously treated with a YB-0158 (vs. DMSO control) (**Figure.11A**). Thus, I observed that YB-0158-treated primary organoids had a significantly lower tumor-initiating capacity when plated in a secondary assay (**Figure.11D, F**). Overall, these experiments confirm to potential of the new ICG/CWP analog YB-0158 to restrict tumor-initiating functions in colorectal cancer, which represents a key hallmark of CSCs.

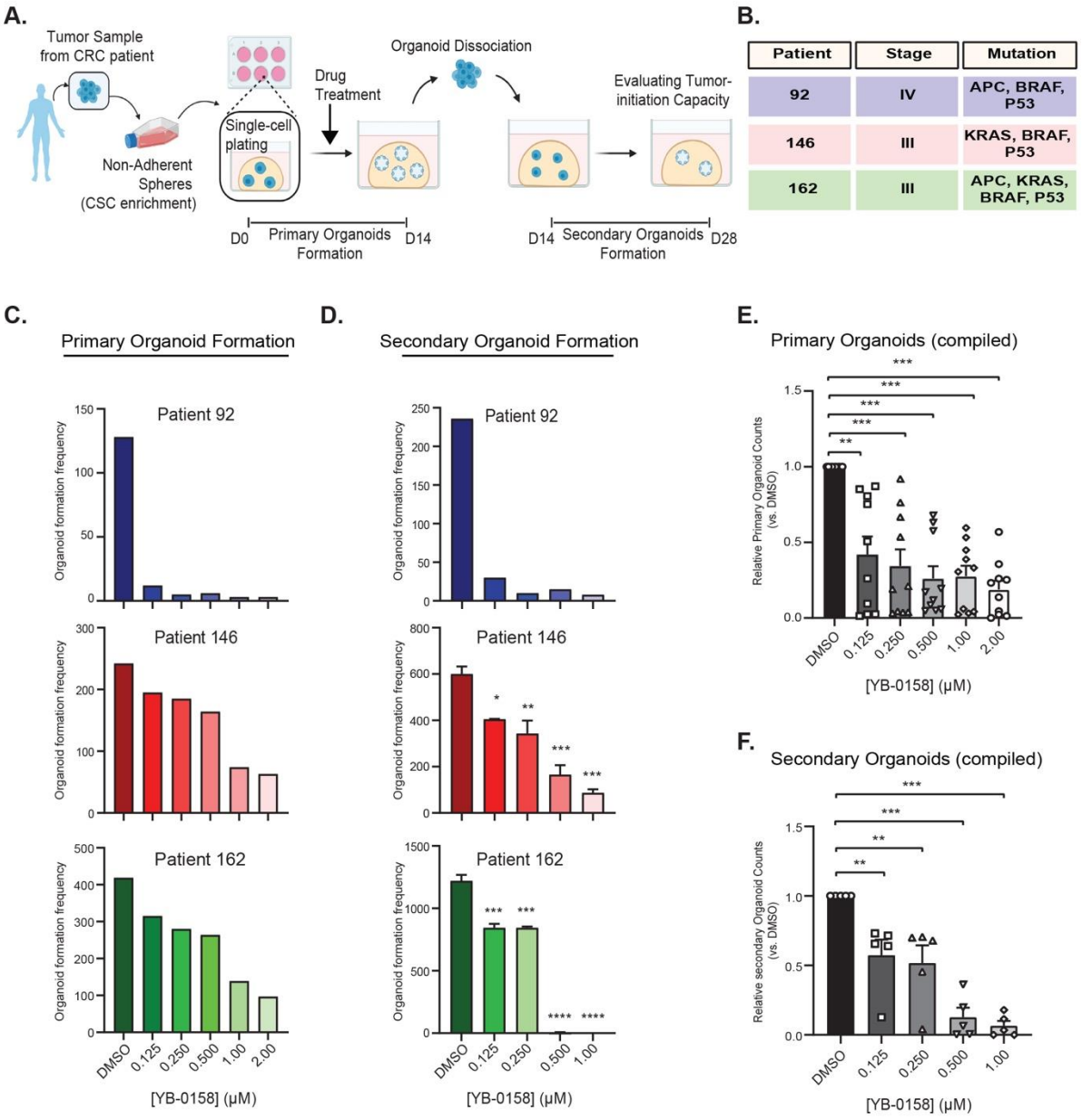

Figure 11. YB-0158 blocks tumor-initiating capacity in primary colorectal cancer patient samples

A) Schematic representation of serial organoid formation assay using primary human colorectal tumor tissues. Cancer stem cell (CSC) fraction is enriched in non-adherent spheroid cultures.

B) Table of clinical information for colorectal cancer patients involved in this study.

C) Patient-specific response in primary organoid formation assays for YB-0158-treated primary samples vs. DMSO controls (#92: n=1, #146: n=5, #162: n=4).

D) Patient-specific response in secondary organoid formation assays for YB-0158-treated primary samples vs. DMSO controls (*: p=0.0298, **: p=0.0097, ***: p<0.0001, ****: p<0.00001).

E) Compiled primary organoid formation frequency observed upon YB-0158 treatments (increasing doses from 0.125 µM to 2 µM, 7 days). Organoid counts were normalized vs. DMSO controls (three patients, n=10, **: p<0.01, ***: p < 0.0001).

F) Compiled organoid formation frequencies observed in secondary plating assays, for DMSO and YB-0158 (0.125 to 1µM) treated groups. Organoid counts were normalized vs. DMSO controls (three patients, n=5, **: p<0.01; ***: p<0.0001).

4.7- YB-0158 is targeting colorectal cancer stem cell activity in vivo

As a next critical step to my project, I sought to determine the potential of YB-0158 to eliminate CCSCs in vivo, within a robust pre-clinical setup. Thus, I used a murine serial tumor transplantation models, which is the gold standard method to measure CSC function *in vivo* (Benoit et al., 2017)). Human-to-mouse and mouse-to-mouse serial tumor transplantation assays were previously shown to be suitable to study human colon CSC activity in response to drug treatments(Le et al., 2009). Akin to serial PDO assays, the detection of a tumor graft in untreated secondary mouse recipients indicates the presence of active CSC populations (**Figure 12A**). To assess the impact of YB-0158 on CCSCs in an immunocompetent *in vivo* context, our lab established a syngeneic mouse model of serial transplantation using the colon adenocarcinoma MC38 cell line (C57BL/6) (**Figure 12A**). MC38 cells can form tumors when injected in the flank of animals from the same genetic background and were previously used to study colorectal tumor immunogenic phenomenon *in vivo* (Jinushi et al., 2011). In previous experiments, we identified that 5 x10^5 MC38 cells per injection site in C57BL/6 mice was optimal to establish robust tumor growth. Upon establishment of the tumor grafts (day-1 to day-7), I performed daily IP injections of YB-0158 and control saline in primary tumor recipients over a period of 14 days. CWP232228 was also tested in the same experimental context as a point of reference and to determine if YB-0158 has a more promising clinical potential than its closely related analog. Based on previous *in vivo* experiment using CWP232228, I fixed the daily experimental dose injected in primary mouse recipients at 100mg/kg for both ICG/CWP analogs(Benoit et al., 2017). Upon 14 days of treatment, residual tumor cells were harvested (day-21) for re-transplantation into secondary murine recipients. The detection of a tumor graft in secondary recipients after experimental day-

36 indicates the presence of active CSCs. The full *in vivo* experimental outline is illustrated in **Figure 12A**.

Before executing the serial tumor transplantation protocol, I determine the potency of both, YB-0158 and CWP232228 on MC38 cell growth inhibition. As in human colorectal cancer cell lines, YB-0158 exhibited a lower EC50 compared to CWP232228 (1.64μM vs. 3.47μM) (**Figure 12B**). Tumor volume was calculated in YB-0158 and CWP232228 treated primary recipients at day-21 upon caliper measurements, and data were compared with tumor size in respective saline control littermates. We observed no changes in tumor volume within primary recipients following 14 days of YB-0158 or CWP232228 vs. control animals (**Figure 12C**). However, I observed a significant decrease of secondary tumor formation in secondary recipients for both YB-0158 and CWP232228 (**Figure 12D**). This was visualized at day-36 by *in vivo* live tumor imaging using an IVIS Spectrum In Vivo Imaging System, upon intravenous injection of 10 nmoles of IRDye-800CW-2-deoxyglucose (IR800-2-DG) fluorescence probe (**Figure 12D**). I also observed that YB-0158 eradicated CCSC activity, and therefore secondary tumor formation in 69% of biological replicates (11/16), while only 45% of CWP232228-treated tumor cell engraftments showed absence of CCSC activity (9/20) (**Figure 12D**). Additional animals will need to be tested to get such a difference between the two analogs to be statistically significant. I also observed that residual secondary tumors from YB-0158-treated group were significantly smaller vs. matched saline controls, while such was not seen in secondary recipients from the CWP232228 group (**Figure 12E**). This represents another indication that YB-0158 has a superior clinical potential than its closely related structural analogs to target CCSC activity.

In previous sections, I described a phenomenon of selective-toxicity toward cancer cells versus healthy intestinal progenitor cells observed upon YB-0158 treatments (**Figure 9**). Thus, I investigated for potential effects of YB-0158 *in vivo* treatment in normal mouse intestinal mucosa. Healthy small intestine (distal ileum) was collected from saline control and YB-0158-treated primary mouse recipients, and histological sections were generated from paraffin-embedded tissues. Next, immunofluorescence staining of E-Cadherin (E-Cad: adherens junctions in epithelial cells), alpha smooth muscle actin (α-SMA: myofibroblasts), and Ki67 (proliferative cells) were performed of tissues from both experimental groups to identify potential drug-induced modifications of the intestinal mucosa architecture and dynamics. Such an exercise revealed that YB-0158-treated animals presented significantly shorter villus compartments and increased number of actively cycling cells within crypt compartments (**Figure 12F, G**). I also observed a thickening of the *muscularis mucosae* in the ileum of YB-0158 treated animals vs. controls (**Figure 12F**), but additional α-SMA immunostaining experiments will be necessary to confirm the statistical validity of such an observation. Although no major defects were observed in the intestine of drug-treated animals, my observations suggest the occurrence of a certain degree of stress exerted by the pharmacological agent on normal epithelial cells. Additional investigations on other organs and systems would strengthen knowledge of toxicology parameters for this new ICG/CWP molecule.

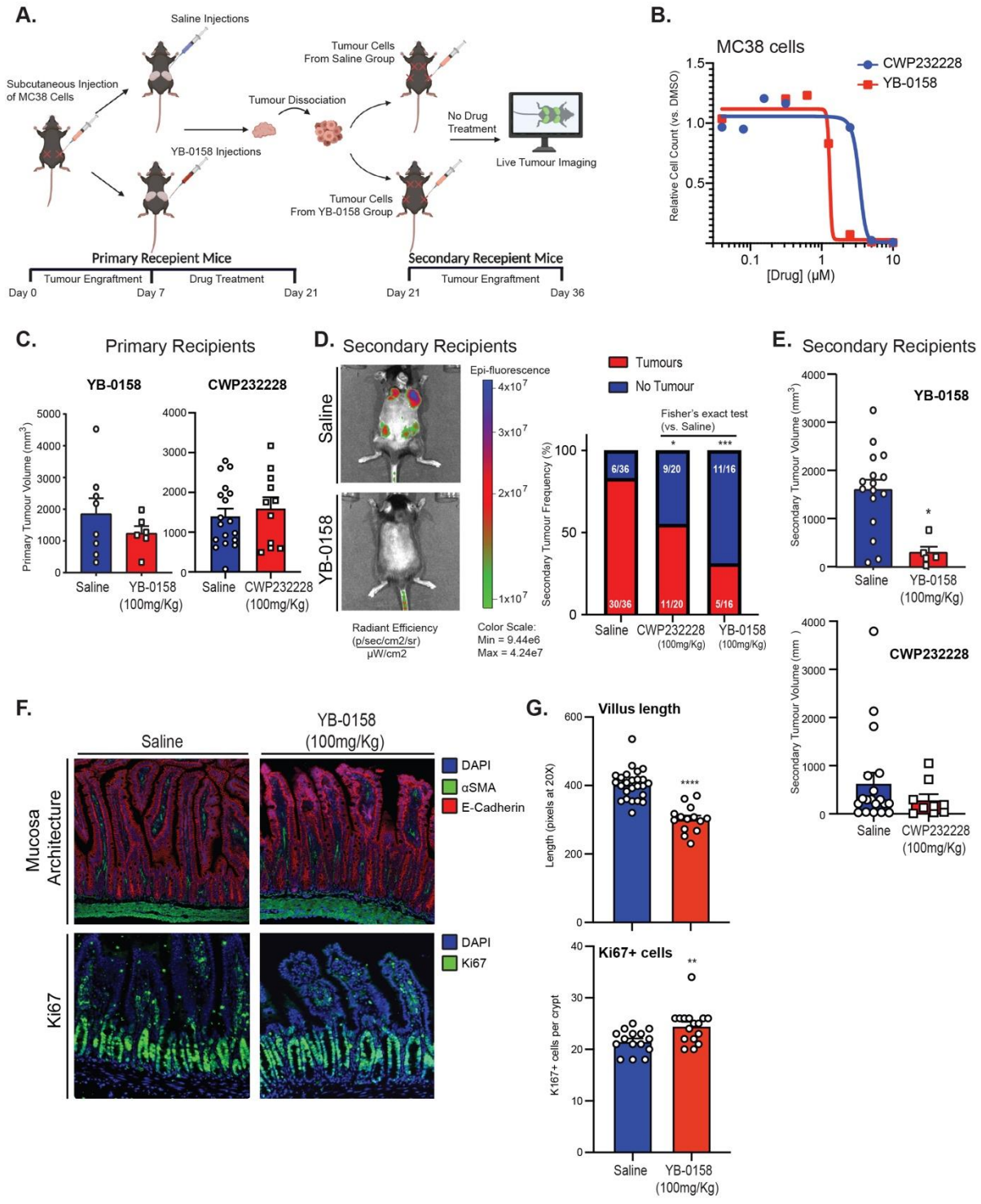

Figure 12. YB-0158 is targeting colorectal cancer stem cell activity in vivo

A) Schematic representation of the murine syngeneic serial tumor transplantation assay used to measure CSC activity *in vivo*. Only primary mouse recipients are treated with YB-0158 or CWP232228. Presence/absence of secondary tumor formation is determined by IVIS live fluorescence tumor imaging.

B) Dose-response experiment assessing growth inhibition caused by peptidomimetics analogs CWP232228 and YB-0158 in murine adenocarcinoma MC38 cells (n=3, 48h).

C) Tumor volume (mm^3) from animals treated with YB-0158 (100mg/kg, n=8), CWP232228 (100mg/kg, n=11), or control saline at day-21 post-engraftment.

D) Frequency of secondary tumors observed in YB-0158, CWP232228, and control saline groups upon day-36. Representative live tumor fluorescence images are shown for saline and YB-0158 treated animals (Fisher's exact test: drug vs. saline, *: p=0.03, ***: p=0.0004).

E) Volume of residual tumors (mm^3) detected in secondary mouse recipients transplanted with cells from YB-0158, CWP232228, and control saline groups. Measures were taken 15 days post-secondary engraftment (experimental day-36) (*: p=0.0036).

F) Representative immunofluorescence imaging of general tissue architecture (E-cadherin, alpha-smooth muscle actin), and crypt proliferative zone (Ki67) in small intestine of mice treated with YB-0158 (100mg/kg, 14 days) or control saline (magnification 20X).

G) Average villus length ($n \geq 14$) and number of Ki67-positive cells per crypt (n=15) in ileum of mice treated with YB-0158 (100mg/kg, 14 days) or control saline (**: p=0.008, ****: p<0.00001).

Chapter 5

Discussion

This project investigates the role of Sam68 in mediating the efficiency of peptidomimetic compounds to successfully target CSCs. Herein, I introduced YB-0158, a more potent ICG/CWP molecule, and describe the potential interaction sites between ICG/CWP molecule and Sam68 proline rich region resulting in the disruption of the cytoplasmic protein-protein interaction between Sam68 and SRC. The abundancy of nuclear Sam68 promotes its association with its co-interactor, CBP, preventing CBP's recruitment on the chromatin site and disrupting CBP/β-catenin interaction, an essential effector of the canonical and often oncogenic WNT pathway, ultimately halting CSC self-renewal. Recent studies postulated that the WNT pathway poses a targetable avenue to develop treatments to suspend the self-renewal CSCs possess (Kahn, 2014; Sebio et al., 2014; Takebe et al., 2015; Yang et al., 2016). However, targeting the WNT pathway may cause lethality for healthy stem cells and disrupt cell homeostasis, which poses problems targeting CSCs.

5.1 ICG/CWP molecules target Sam68 resulting to their anti-neoplastic effect

The WNT/β-catenin pathway is highly involved in the stem cell maintenance for somatic tissues as well as CSCs survival. The pharmacological targeting of the WNT/β-catenin pathway has been an avenue for drug development to disrupt the self-renewal capacity of CSCs through decrease

expression of β-catenin/TCF related genes (Kahn, 2014; Sebio et al., 2014; Takebe et al., 2015; Yang et al., 2016). Since CBP is highly recruited to β-catenin/TCF chromatin region for increased transactivation of self-renewal genes, pharmacological inhibition of CBP's HAT activity has been a druggable target for potential cancer treatments (Bowers et al., 2010; Conery et al., 2016a; Kahn, 2014; Ma et al., 2005; Miyabayashi et al., 2007b). CBP HAT inhibitors, C646 and I-CBP112, successfully suppress cellular proliferation (Bowers et al., 2010; Conery et al., 2016a). In contrast, our study displays the increased efficacy of ICG/CWP molecule via decreasing cellular proliferation and promoting cellular differentiation **(Figure 5 C-D)**. ICG/CWP molecules have been shown to bind to CBP for the downregulation of β-catenin/TCF responsive genes through the disruption of CBP/ β-catenin interaction (Emami et al., 2004). By contrast, a recent study by Benoit *et al,* suggests the involvement of Sam68 in facilitating the disruption of CBP/ β-catenin complex (Benoit et al., 2017). My study further validates that indeed, ICG/CWP molecules target Sam68 instead of CBP, contributing to its anti-neoplastic effect. As seen in our pull-down assay, CWP232228 physically interacts with Sam68 to drastically reduce cellular proliferation, in expense to promotion of differentiation without altering CBP, and Sam68 protein levels **(Figure 5C, G)**. Sam68 is indeed a key mediator for ICG/CWP drug efficiency, however, the mechanism in which ICG/CWP and Sam68 function remains unknown.

5.2 ICG/CWP molecule disrupts the SRC/Sam68 cytoplasmic interaction

Sam68 is known to play roles in RNA splicing, transcription, and signalling (Bielli et al., 2011; Frisone et al., 2015). With its great involvement in cellular processes, aberrant levels of Sam68

poses disturbances in regular cellular processes. In fact, high levels of Sam68 is correlated with cancer progression and adverse prognosis (Bielli et al., 2011; Busà et al., 2007; Song et al., 2010). Notably, cytoplasmic tyrosine phosphorylation of Sam68 by SRC is frequently seen in cancer, making this an ideal pharmacological target (Busà et al., 2007; Taylor et al., 1995). Sam68 proline rich regions (P3-P5) are known to interact with the SH3 domain of SRC, displayed by UCS15As ability to disrupt Sam68/SRC interaction in this region (Oneyama et al., 2002; Taylor et al., 1995; Taylor and Shalloway, 1994). Our gathered *in silico* docking data displayed UCS15A and ICG001 share common interaction sites with Sam68 (**Figure 6B)**, further suggesting that ICG/CWP molecules are direct Sam68 interactors.

5.3 Identification of more potent ICG/CWP class molecules is required to effectively target CSCs

ICG/CWP molecules are currently on phase IA/IB clinical trials with modest effects (Ko et al., 2016). However, trials have been terminated with no further details disclosed (Ko et al., 2016). Such clinical failure highlights the importance of identifying new CWP analogs with greater efficacy and selectivity. Different ICG/CWP structures were attained based on structural changes to three different side chains (A, B) (**Figure 6D-G**). ICG/CWP analogs were docked in the proline-rich domains of Sam68, which is known binding site of UCS15A (Oneyama et al., 2003; Oneyama et al., 2002). Thus, ICG/CWP analogs were virtually docked in the proline-rich domain and generated a predicted binding affinity (Keq) for each molecule **(Figure 6E)**. YB-0159 emerges with

a better binding affinity (Keq) than UCS15A and CWP232904 **(Figure 6G)**. Interestingly, UCS15A, CWP232228 and YB-0158 all interact with common residues such as GLY305, in the proline rich region of Sam68 **(Figure 6B and 7C).** Notably, YB-0159 shares a similar structure to its derivative CWP compound with one methyl group different **(Figure 6H).** Indeed, that the lack of one methyl group on site B of YB-0159 has given an advantage to form a hydrogen bond on Sam68 Gly305, which may have contributed to better affinity of YB-0159 with Sam68 in comparison to CWP232904. Based on these results, YB-0159 warrants further investigation throughout this study.

Although the *in silico* docking displayed promising results, further investigation is still required to support this predictive computational binding between Sam68 and ICG/CWP molecule. Such technique will be x-ray crystallography to display the true interaction between Sam68 and YB-0159. Despite this set back, we decided to understand the importance of the GLY 305 in the binding of both CWP232904 and YB-0159 through using mutated Sam68 in the GLY 305 still using in silico docking, precisely that upon introduction of the mutation on GLY305, there is a notable decrease in binding affinity of YB-0159 **(Figure 7 D, E).** This suggests that upon changes to the ICG/CWP molecular structure by one methyl group on site B, these compounds have the potential to yield a peptidomimetic molecule with greater binding affinity towards Sam68. Moreover, it further validates the importance of GLY305 in the interaction between Sam68 and ICG/CWP molecule. Yet, for future studies, generating cellular culture harbouring mutated Sam68 and perform drug treatment to display the drug effectivity will further validate this result.

5.4 YB-0158 effectively promotes Sam68 nuclear accumulation to disrupt transactivation of CBP/β-catenin genes

CWP232228 is known to decrease self-renewal capacity of AML (Benoit et al., 2017) Since CWP232228 and YB-0158 differ with one methyl group, we therefore predict that YB-0158 will have similar biological activity as its parental molecule. In comparison, both molecules have the ability to affect pluripotency of t-hESCs **(Figure 8C)**, yet YB-0158 is more effective in decreasing t-hESCs and HT29 cell counts at lower doses **(Figure 8A)**. In addition, YB-0158 drug dose treatment of t-hESCs revealed YB-0158 shows enhanced Sam68 nuclear localization compared to CWP232228 **(Figure 8F,G)**. In fact, YB-0158 disrupts the interaction between cytoplasmic Sam68/SRC protein-protein interaction **(Figure 8D)** without affecting the overall SRC phosphorylation ability **(Figure 8E)**. These results support that YB-0158-mediated cytotoxicity is significantly correlated with Sam68 nuclear accumulation, which is the after-effect upon the disruption of Sam68/SRC cytoplasmic interaction, perhaps, through the disruption of Sam68/SRC complex causes a nuclear shift of Sam68. Although, further studies are still required to fully understand the nuclear shift of Sam68 in the presence of ICG/CWP molecule, which is likely to occur through Sam68 SUMOylation (Benoit et al., 2017). Collectively, CWP has the ability to promote nuclear accumulation of Sam68 in AML leading to decreased in tumorigenesis as previously been disclosed (Benoit et al., 2017).

Co-localization of Sam68, either cytoplasmic with SRC or nuclear with CBP, displays a relationship to cancer progression. In renal carcinoma high Sam68 levels are localized to the cytoplasm and correlate with poor prognosis (Zhang et al., 2009). Comparatively, normal cells have high abundance of Sam68, which is required by multiple signalling pathway for proper

cellular regulation. Possibly, Sam68 cytoplasmic localization contributes to cancer progression through enhancing mRNA splicing events and participating in multiple cellular signalling (Bielli et al., 2011). Thus, facilitating the localization of Sam68 to inhibit transcription is one great away to counter-act the promotion of cancer. Through the use of the small molecule, YB-0158, both inhibits SRC/Sam68 interaction and promotes Sam68 nuclear localization leading to cytotoxicity in colorectal cancer cells. Interestingly, increased Sam68 nuclear localization seems to prevent CBP localization in the chromatin, which results in the repression of WNT/β-catenin transcriptional expression **(Figure 8F,H, 10C)**. CBP/Sam68 interaction results in the repressive transcription of CBP mediated gene-expression (Hong et al., 2002a). This further supports the postulated complex formation of CBP/Sam68 to disrupt the CBP/ β-catenin interaction resulting to an antineoplastic effect (Benoit et al., 2017).

Sam68's high involvement in cellular processes is advantageous for the efficiency of ICG/CWP molecules. Based on our results, overexpression of Sam68 is evidently seen across highly tumorigenic colorectal cancer cell lines compared to normal epithelial cells, as well as, in primary CRC patients **(Figure 9A,B).** Drug-dose response treatment across these cell lines exhibited a selective targeting in highly tumorigenic cells while sparring normal epithelial cells **(Figure 9C)**. Interestingly, dose-response assays present a lower selective toxicity ratio for YB-0158 compared to CWP232228, a measure of relative toxicity to malignant cells compared to healthy cells, indicating that YB exhibits enhanced potency against cancerous cells with no change in toxicity to healthy cells, as compared to CWP232228 **(Figure 9C)**. Moreover, YB-0158 functions through decreasing cellular proliferation and increasing the number of cells undergoing apoptosis **(Figure 10A, B).** As expected, YB-0158 has the capacity to downregulate WNT/β-catenin

associated genes such as *sox9, lgr5* and *survivin*. These results corroborate YB-0158 as a more potent and effective anti-cancerous molecule and represents the molecule used further investigation.

Conventional chemotherapeutics failed to target CSCs, providing the seeds of metastasis and tumour recurrence. Therefore, to prevent tumour recurrence and metastasis, there is an urgent need to identify small molecules selectively targeting and eradicating CSCs. CWP232228 has been reported to effectively inhibit WNT activity, resulting in a decrease in the tumour-initiating capacity of breast cancer and AML cells (Benoit et al., 2017; Jang et al., 2015). New technological assays have recently been developed to assess the tumour-initiating capacity of CSCs after drug treatment. The serial PDO assay allows CSCs to recapitulate 3D tumor structures grown in culture plates, allowing a more representative model for assessing the impact of small molecules on the tumor-initiating capacity of these cells. (Tuveson and Clevers, 2019). Interestingly, our data demonstrates that treatment with YB-0158 in primary organoids effectively decreases organoid counts compared to DMSO, indicating a reduction in viable CSCs following drug treatment **(Figure 11C,E)**. This observation was strengthened through the use of a secondary organoid formation assay (in the absence of drugs) where YB-0158 treated organoids resulted in reduced organoid formation frequencies **(Figure 11D,F)**. Undeniably, this is indicative of YB-0158 treatment reducing the CSC populations that are first enriched via sphere formation. Collectively, YB-0158 treatment on primary patient samples is selective in targeting tumor-initiating capacity as identified through 3D organoid formation assays.

To fully assess the biological activity in the presence of other external factors such as response to the immune system and tumor microenvironment, a murine syngeneic model was used. Upon

treatment of primary recipient mice bearing tumours, we detected no differences in tumour volume between Saline (control) and YB-0158 treated mice **(Figure 12C, D)**. Following 11 days of drugs vs. control treatment, tumours were extracted from primary recipient mice and transferred to secondary recipient mice to study the impact of drug treatment on CSC populations. Secondary tumor formation frequency was reduced in YB-treated mice compared to vehicle control **(Figure 12E).** In addition, tumour volume in YB-0158 treated mice were significantly smaller than those from saline treated mice **(Figure 12E).** Collectively, these findings demonstrated that YB-0158 inhibits the self-renewal capacity of a murine syngeneic model and decreases tumour growth. Interestingly, when comparing YB-0158 treated mice to CWP232228 treatment mice, YB-0158 showed an enhanced anti-tumor response, consistent with other experiments. **(Figure 12 D)**, Moreover, YB-0158 does not jeopardize cell regulation of normal stem cells **(Figure 12F)**. Indeed, the use of syngeneic serial tumour transplantation is crucial, as tumour initiation frequency is highly indicative of the functional capacity of CSCs, while impaired tumour initiation upon secondary implantation indicates impaired CSC function which is seen in the Saline treated mice **(Figure 12).**

Overall, our results suggest that YB-0158 effectively targets CSCs activity *in vivo*. Compelling *ex vivo* and *in vivo* evidences demonstrated that YB-0158 possesses the ability to inhibit the self-renewal capacity of CSCs, leading to decreased tumour recurrence and tumour progression after drug treatment.

Chapter 6

Conclusion and Future Directions

Overall, this project unveils YB-0158, a more potent ICG/CWP anti-CSC compound that demonstrates significant selective toxicity toward cancer vs. healthy cells. YB-0158 drug effectivity demonstrates notable reliance on the nuclear interaction of Sam68 with CBP and subsequent disruption of CBP/B-catenin complex formation, a key effector of WNT signalling. Moreover, through targeting Sam68, YB-0158 avoids toxicity caused by nonspecific WNT inhibition in healthy stem cells. Furthermore, this project elucidates the important role of Sam68 and that Sam68/SRC is a potential avenue for novel anti-cancer compounds, which can specifically target CSCs.

However, there are still a lot of remaining questions that are unanswered, which can potentially be room for future studies. The full mechanism of action of YB-0158 interaction with Sam68 is still not fully elucidated, such that the missing link from disruption of Sam68/SRC interaction to Sam68 nuclear localization and a broader aspect of the gene regulation upon treatment. As well as, its YB-0158/Sam68 interaction can be shown through the use of x-ray crystallography.

Future investigations on therapeutically targeting Sam68 may potentially avoid killing healthy cells and eradicate CSCs. Such that, inhibitors like YB-0158 may potentially have a higher chance of passing clinical trials. Moreover, further investigations are required to target other subsets of cancer and to study combination therapy that can target different epigenetic

signatures and genetic signatures. Critically, this study presents a novel, promising ICG/CWP class compound that demonstrates substantial pre-clinical anti-CSC activity.

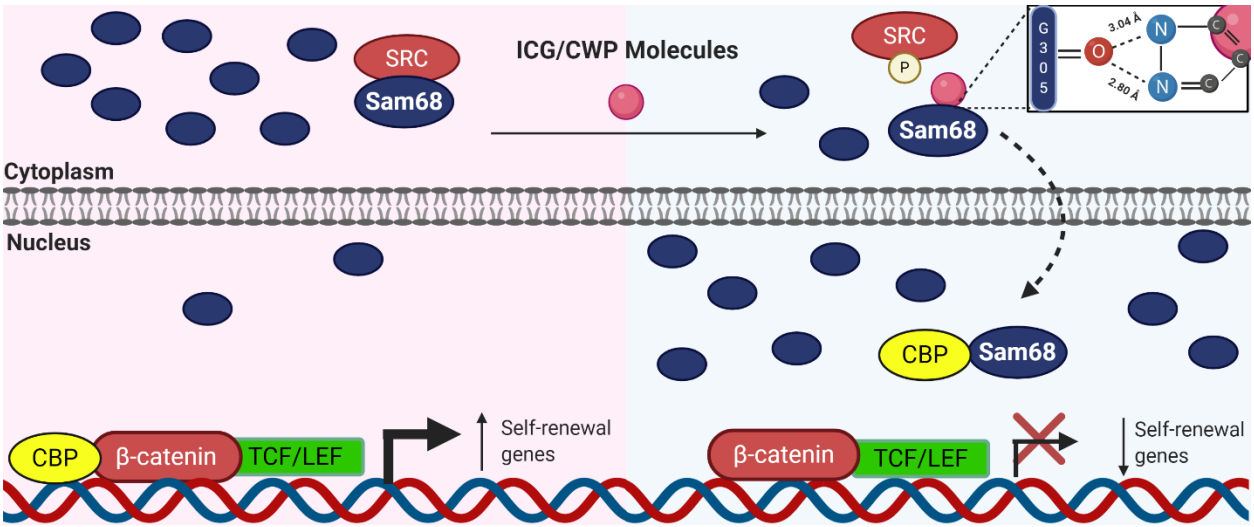

Figure 13. Schematic Conclusion of Thesis.

Appendices

Table 3. List of Cell lines and Mice

Cell lines and mice		
Reagent	Source	Identifier
HIEC	ATCC	CRL-3266
SW480	ATCC	CCL-228
HT29	ATCC	HTB-38
HCT116	ATCC	CCL-247
MC38	Kerafast	ENH204-FP
HEK293-FT	Thermo Fisher Scientific	R70007
C57/BL6 female mice	Charles River	Strain code: 027
Transformed human embryonic stem cells	A gift from Dr. Mickie Bhatia, McMaster University (Werbowetski-Ogilvie et al., 2009)	

Table 4. List of Chemicals and Reagents

Chemicals and Reagents		
Reagent	Source	Identifier
CWP232228	MedChem Express	HY-18959
ICG-001	Tocris Bioscience	4505
YB-0158	Haoyuan Chemexpress	N/A
PRI-724	MedChemExpress	142225-38-0
DMSO	ATCC	CA95040-114L
Matrigel	Stem Cell Technologies	
Fetal Bovine Serum	Wisent BioProduct	080-450
Polybrene Transfection Reagent	Millipore Sigma	TR-1003-G
Lipofectamine LTX Reagent	Invitrogen	15338500
McCoy's 5A Medium	Lonza	
OptiMEM reduced media	Gibco	31985-070
DMEM/ High Glucose media	Hyclone	SH30243.01
Leibovitz's L-15 Medium	Gibco	11415-064
Epithelium growth factor	Wisent Bioproducts	511-110-EU
HEPES	Gibco	15630-080
L-glutamine	Gibco	35050-061
Fetal Bovine Serum qualified Canada Origin (FBS)	Thermofisher	12483-020
HBSS	Gibco	14170-120
Collagenase IV	Stem Cell Technologies	07909
1X TrypLE Express Enzyme	ThermoFisher	12605-010
Tween-20	Fisher	BP151-100
Marker GE Amersham ECL Full-Range Rainbow Ladder	VWR	CA95044-114L
FBS Premium Quality	Wisent	080-450

Table 5. List of Commercial Assay

Commercial Assay		
Reagent	Source	Identifier
Total RNA Purification kit	Norgen BIOTEK	37500
Power-up Syber Green Master mix	Thermo Fisher	A25742
SuperScript VILO cDNA Synthesis Kit	Invitrogen	11754050
Immobilon Western Chemiluminescent HRP substrate	Millipore	WBKLS0500
BD Cytofix/Cytoperm kit	BD Bioscience	554714
EDU proliferation kit (iFluor 488)	Abcam	Ab219801
CellEvent Caspase 3/7	Thermofisher	C10423
QIAprep spin Miniprep Kit	Qiagen	27104
VectaShield Antifade Mounting Medium with Dapi	VectaShield	H-1200
Fixation/Permeabilization Solution Kit	BD Cytofix/Cytoperm™	554714
Syringe Driven Filter Unit	Millex	SLH V033RS
Chromatin IP Purification Kit	Active Motif	58002

Table 6. List of Lentiviral Plasmids

Lentiviral Plasmid		
Plasmid	Source	Identifier
pPAX.2	Addgene	12260
pMD2.G	Addgene	12259
Sam68 - 44	Millipore Sigma	NM_006559.x-2443s1c1
Sam68 – 45	Millipore Sigma	NM_006559.x-872s1c1
Sam68 - 46	Millipore Sigma	NM_006559.x-481s1c1
Sam68 – 428104	Millipore Sigma	NM_006559.1-1519s21c1
Sam68 – 428752	Millipore Sigma	NM_006559.1-1245s21c1
CBP – 6846	Millipore Sigma	NM_004380.1-3884s1c1
CBP – 11027	Millipore Sigma	NM_004380.1-1161s1c1
CBP – 356053	Millipore Sigma	NM_004380.2-2144s21c1
CBP – 356081	Millipore Sigma	NM_004380.2-777s21c1
CBP – 356082	Millipore Sigma	NM_004380.2-4548s21c1

References

Arnold, M., Sierra, M.S., Laversanne, M., Soerjomataram, I., Jemal, A., and Bray, F. (2017). Global patterns and trends in colorectal cancer incidence and mortality. Gut *66*, 683-691.

Babic, I., Jakymiw, A., and Fujita, D.J. (2004). The RNA binding protein Sam68 is acetylated in tumor cell lines, and its acetylation correlates with enhanced RNA binding activity. Oncogene *23*, 3781-3789.

Batlle, E., and Clevers, H. (2017). Cancer stem cells revisited (Nature Publishing Group), pp. 1124-1134.

Behrens, J., and Lustig, B. (2004). The Wnt connection to tumorigenesis. The International Journal of Developmental Biology *48*, 477-487.

Ben-Porath, I., Thomson, M.W., Carey, V.J., Ge, R., Bell, G.W., Regev, A., and Weinberg, R.A. (2008). An embryonic stem cell-like gene expression signature in poorly differentiated aggressive human tumors. Nature Genetics *40*, 499-507.

Benoit, Y.D., Guezguez, B., Boyd, A.L., and Bhatia, M. (2014). Molecular Pathways: Epigenetic Modulation of Wnt-Glycogen Synthase Kinase-3 Signaling to Target Human Cancer Stem Cells. Clin Cancer Res *20*.

Benoit, Y.D., Mitchell, R.R., Risueño, R.M., Orlando, L., Tanasijevic, B., Boyd, A.L., Aslostovar, L., Salci, K.R., Shapovalova, Z., Russell, J.*, et al.* (2017). Sam68 Allows Selective Targeting of Human Cancer Stem Cells. Cell Chemical Biology *24*, 833-844.e839.

Bergin, C.J., Zouggar, A., Haebe, J.R., Masibag, A.N., Desrochers, F.M., Reilley, S.Y., Agrawal, G., and Benoit, Y.D. (2020). G9a controls pluripotent-like identity and tumor-initiating function in human colorectal cancer. Oncogene.

Bielli, P., Busà, R., Paronetto, M.P., and Sette, C. (2011). The RNA-binding protein Sam68 is a multifunctional player in human cancer. Endocrine-Related Cancer *18*.

Bonnet, D., and Dick, J.E. (1997). Human acute myeloid leukemia is organized as a hierarchy that originates from a primitive hematopoietic cell. Nature medicine *3*, 730-737.

Bowers, E.M., Yan, G., Mukherjee, C., Orry, A., Wang, L., Holbert, M.A., Crump, N.T., Hazzalin, C.A., Liszczak, G., Yuan, H.*, et al.* (2010). Article Virtual Ligand Screening of the p300 / CBP Histone Acetyltransferase : Identification of a Selective Small Molecule Inhibitor. Chemistry & Biology *17*, 471-482.

Brenner, H., Kloor, M., and Pox, C.P. (2014). Colorectal cancer. The Lancet *383*, 1490-1502.

Bs, K., Lee, S.H., Kim, J.M., Huang, S., Kim, S.H., Rho, Y.S., Bae, W.J., Kang, H.J., Kim, Y.S., Moon, J.H.*, et al.* (2015). Oct4 is a critical regulator of stemness in head and neck squamous carcinoma cells. Oncogene *34*, 2317-2324.

Busà, R., Paronetto, M.P., Farini, D., Pierantozzi, E., Botti, F., Angelini, D.F., Attisani, F., Vespasiani, G., and Sette, C. (2007). The RNA-binding protein Sam68 contributes to proliferation and survival of human prostate cancer cells. Oncogene *26*, 4372-4382.

Chan, H.M., and La Thangue, N.B. (2001). p300/CBP proteins: HATs for transcriptional bridges and scaffolds | Journal of Cell Science, pp. 2363-2373.

Chen, Z., He, X., Jia, M., Liu, Y., Qu, D., Wu, D., Wu, P., Ni, C., Zhang, Z., Ye, J.*, et al.* (2013). β-catenin Overexpression in the Nucleus Predicts Progress Disease and Unfavourable Survival in Colorectal Cancer: A Meta-Analysis. PLoS ONE *8*, e63854-e63854.

Conery, A.R., Centore, R.C., Neiss, A., Keller, P.J., Joshi, S., Spillane, K.L., Sandy, P., Hatton, C., Pardo, E., Zawadzke, L.*, et al.* (2016a). Bromodomain inhibition of the transcriptional coactivators CBP/EP300 as a therapeutic strategy to target the IRF4 network in multiple myeloma. eLife *5*.

Conery, A.R., Centore, R.C., Neiss, A., Keller, P.J., Joshi, S., Spillane, K.L., Sandy, P., Hatton, C., Pardo, E., Zawadzke, L.*, et al.* (2016b). Correction: Bromodomain inhibition of the transcriptional coactivators CBP/EP300 as a therapeutic strategy to target the IRF4 network in multiple myeloma. Elife *5*.

Cortes, J.E., Faderl, S., Pagel, J., Jung, C.W., Yoon, S.-S., Koh, Y., Pardanani, A.D., Hauptschein, R.S., Lee, K.-J., and Lee, J.-H. (2015). Phase 1 study of CWP232291 in relapsed/refractory acute myeloid leukemia (AML) and myelodysplastic syndrome (MDS). Journal of Clinical Oncology *33*, 7044-7044.

Crespo, M., Vilar, E., Tsai, S.-Y., Chang, K., Amin, S., Srinivasan, T., Zhang, T., Pipalia, N.H., Chen, H.J., Witherspoon, M.*, et al.* (2017). Colonic organoids derived from human induced pluripotent stem cells for modeling colorectal cancer and drug testing. Nature Medicine *23*, 878-884.

Dalerba, P., Dylla, S.J., Park, I., Liu, R., Wang, X., Cho, R.W., Hoey, T., Gurney, A.L., Huang, E.H., Simeone, D.M.*, et al.* (2007). Phenotypic characterization of human colorectal cancer stem cells. Proc Nat Acad Sci, USA *104 no 24*, 10158-10163.

Dallakyan, S., and Olson, A. (2015). Small-Molecule Library Screening by Docking with PyRx. Methods in molecular biology (Clifton, NJ) *1263*, 243-250.

de Sousa e Melo, F., Kurtova, A.V., Harnoss, J.M., Kljavin, N., Hoeck, J.D., Hung, J., Anderson, J.E., Storm, E.E., Modrusan, Z., Koeppen, H.*, et al.* (2017). A distinct role for Lgr5+ stem cells in primary and metastatic colon cancer. Nature *543*, 676-680.

Emami, K.H., Nguyen, C., Ma, H., Kim, D.H., Jeong, K.W., Eguchi, M., Moon, R.T., Teo, J.-l., Oh, S.W., Kim, H.Y*., et al.* (2004). A small molecule inhibitor of beta catenin/creb binding protein transcription. PNAS *101*.

Fevr, T., Robine, S., Louvard, D., and Huelsken, J. (2007). Wnt/-Catenin Is Essential for Intestinal Homeostasis and Maintenance of Intestinal Stem Cells †. MOLECULAR AND CELLULAR BIOLOGY *27*, 7551-7559.

Forli, S., Huey, R., Pique, M.E., Sanner, M.F., Goodsell, D.S., and Olson, A.J. (2016). Computational protein-ligand docking and virtual drug screening with the AutoDock suite. Nature Protocols *11*, 905-919.

Freedman, S.J., Sun, Z.Y.J., Poy, F., Kung, A.L., Livingston, D.M., Wagner, G., and Eck, M.J. (2002). Structural basis for recruitment of CBP/p300 by hypoxia-inducible factor-1α. Proceedings of the National Academy of Sciences of the United States of America *99*, 5367-5372.

Frisone, P., Pradella, D., Matteo, A.D., Belloni, E., Ghigna, C., and Paronetto, M.P. (2015). SAM68: Signal Transduction and RNA Metabolism in Human Cancer.

Gabata, R., Harada, K., Mizutani, Y., Ouchi, H., Yoshimura, K., Sato, Y., Kitao, A., Kimura, K., Kouji, H., Miyashita, T*., et al.* (2020). Anti-tumor Activity of the Small Molecule Inhibitor PRI-724 Against β-Catenin-activated Hepatocellular Carcinoma. Anticancer Research *40*, 5211.

Gaillard, T. (2018). Evaluation of AutoDock and AutoDock Vina on the CASF-2013 Benchmark. Journal of Chemical Information and Modeling *58*, 1697-1706.

Gehart, H., and Clevers, H. (2019). Tales from the crypt: new insights into intestinal stem cells (Nature Publishing Group), pp. 19-34.

Hong, W., Resnick, R.J., Rakowski, C., Shalloway, D., and Taylor, S.J. (2002a). Physical and Functional Interaction Between the Transcriptional Cofactor CBP and the KH Domain Protein Physical and Functional Interaction Between the Transcriptional Cofactor CBP and the KH Domain Protein Sam68. Molecular Cancer Research *01*, 48-55.

Hong, W., Resnick, R.J., Rakowski, C., Shalloway, D., Taylor, S.J., and Blobel, G.A. (2002b). Physical and functional interaction between the transcriptional cofactor CBP and the KH domain protein Sam68. PNAS.

Ilyas, M., Tomlinson, I.P.M., Rowan, A., Pignatelli, M., and Bodmer, W.F. (1997). β-Catenin mutations in cell lines established from human colorectal cancers. Proceedings of the National Academy of Sciences of the United States of America *94*, 10330-10334.

Jang, G.-B., Hong, I.-S., Kim, R.-J., Lee, S.-Y., Park, S.-J., Lee, E.-S., Park, J.H., Yun, C.-H., Chung, J.-U., Lee, K.-J.*, et al.* (2015). Tumor and Stem Cell Biology Wnt/b-Catenin Small-Molecule Inhibitor CWP232228 Preferentially Inhibits the Growth of Breast Cancer Stem-like Cells.

Jinushi, M., Chiba, S., Yoshiyama, H., Masutomi, K., Kinoshita, I., Dosaka-Akita, H., Yagita, H., Takaoka, A., and Tahara, H. (2011). Tumor-associated macrophages regulate tumorigenicity and anticancer drug responses of cancer stem/initiating cells. Proceedings of the National Academy of Sciences *108*, 12425.

Joung, J.G., Oh, B.Y., Hong, H.K., Al-Khalidi, H., Al-Alem, F., Lee, H.O., Bae, J.S., Kim, J., Cha, H.U., Alotaibi, M.*, et al.* (2017). Tumor heterogeneity predicts metastatic potential in colorectal cancer. Clinical Cancer Research *23*, 7209-7216.

Kahn, M. (2014). Can we safely target the WNT pathway? Nature Reviews Drug Discovery *13*, 513-532.

Ko, A.H., Chiorean, E.G., Kwak, E.L., Lenz, H.-J., Nadler, P.I., Wood, D.L., Fujimori, M., Inada, T., Kouji, H., and McWilliams, R.R. (2016). Final results of a phase Ib dose-escalation study of PRI-724, a CBP/beta-catenin modulator, plus gemcitabine (GEM) in patients with advanced pancreatic adenocarcinoma (APC) as second-line therapy after FOLFIRINOX or FOLFOX. Journal of Clinical Oncology *34*, e15721-e15721.

Kreso, A., and Dick, J.E. (2014). Evolution of the cancer stem cell model. Cell Stem Cell *14*, 275-291.

Kreso, A., O'Brien, C.A., Van Galen, P., Gan, O.I., Notta, F., Brown, A.M.K., Ng, K., Jing, M., Wienholds, E., Dunant, C*., et al.* (2013). Variable clonal repopulation dynamics influence chemotherapy response in colorectal cancer. Science *339*, 543-548.

Laskowski, R.A., and Swindells, M.B. (2011). LigPlot+: Multiple Ligand–Protein Interaction Diagrams for Drug Discovery. Journal of Chemical Information and Modeling *51*, 2778-2786.

Le, C., Ramesh, A.V., Flesken-Nikitin, A., Choi, J., and Nikitin, A.Y. (2009). Mouse Models for Cancer Stem Cell Research. Toxicologic Pathology *38*, 62-71.

Lee, D.-W., Han, S.-W., Cha, Y., Bae, J.M., Kim, H.-P., Lyu, J., Han, H., Kim, H., Jang, H., Bang, D*., et al.* (2019). Association of pathway mutation with survival after recurrence in colorectal cancer patients treated with adjuvant fluoropyrimidine and oxaliplatin chemotherapy. BMC Cancer *19*, 421-421.

Lenz, H.J., and Kahn, M. (2014). Safely targeting cancer stem cells via selective catenin coactivator antagonism (Blackwell Publishing Ltd), pp. 1087-1092.

Lima-Fernandes, E., Murison, A., da Silva Medina, T., Wang, Y., Ma, A., Leung, C., Luciani, G.M., Haynes, J., Pollett, A., Zeller, C*., et al.* (2019). Targeting bivalency de-represses Indian Hedgehog and inhibits self-renewal of colorectal cancer-initiating cells. Nature Communications *10*.

Lukong, K.E., and Richard, S. (2007). Targeting the RNA-binding protein Sam68 as a treatment for cancer? , pp. 539-544.

Ma, H., Nguyen, C., Lee, K.S., and Kahn, M. (2005). Differential roles for the coactivators CBP and p300 on TCF/β-catenin-mediated survivin gene expression. Oncogene *24*, 3619-3631.

Miyabayashi, T., Eo, J.L., Yamamoto, M., McMillan, M., Nguyen, C., and Kahn, M. (2007a). Wnt/beta-catenin/CBP signaling maintains long-term murine embryonic stem cell pluripotency. Proceedings of the National Academy of Sciences *104*, 5668-5673.

Miyabayashi, T., Teo, J.-L., Yamamoto, M., McMillan, M., Nguyen, C., and Kahn, M. (2007b). Wnt/-catenin/CBP signaling maintains long-term murine embryonic stem cell pluripotency.

O'Brien, C.A., Pollett, A., Gallinger, S., and Dick, J.E. (2007). A human colon cancer cell capable of initiating tumour growth in immunodeficient mice. Nature *445*, 106-110.

O'Connor, E.S., Greenblatt, D.Y., LoConte, N.K., Gangnon, R.E., Liou, J.-I., Heise, C.P., and Smith, M.A. (2011). Adjuvant Chemotherapy for Stage II Colon Cancer With Poor Prognostic Features. Journal of Clinical Oncology *29*, 3381-3388.

Oneyama, C., Agatsuma, T., Kanda, Y., Nakano, H., Sharma, S.V., Nakano, S., Narazaki, F., and Tatsuta, K. (2003). Synthetic inhibitors of proline-rich ligand-mediated protein-protein interaction: Potent analogs of UCS15A. Chemistry and Biology *10*, 443-451.

Oneyama, C., Nakano, H., and Sharma, S.V. (2002). UCS15A, a novel small molecule, SH3 domain-mediated protein-protein interaction blocking drug. Oncogene *21*, 2037-2050.

Pinto, D., Gregorieff, A., Begthel, H., and Clevers, H. (2003). Canonical Wnt signals are essential for homeostasis of the intestinal epithelium. Genes and Development *17*, 1709-1713.

Punt, C.J.A., Koopman, M., and Vermeulen, L. (2017). From tumour heterogeneity to advances in precision treatment of colorectal cancer (Nature Publishing Group), pp. 235-246.

Resh, M.D. (2008). The Ups and Downs of Src Regulation : Tumor Suppression by Cbp. 2007-2009.

Rizo, A., Dontje, B., Vellenga, E., De Haan, G., and Schuringa, J.J. (2008). Long-term maintenance of human hematopoietic stem/progenitor cells by expression of BMI1.

Sachlos, E., Risueno, R.M., Laronde, S., Shapovalova, Z., Lee, J.H., Russell, J., Malig, M., McNicol, J.D., Fiebig-Comyn, A., Graham, M*., et al.* (2012). Identification of drugs including a dopamine receptor antagonist that selectively target cancer stem cells. Cell *149*, 1284-1297.

Santer, F.R., Höschele, P.P.S., Su, J.O., Erb, H.H.H., Bouchal, J., Cavarretta, I.T., Parson, W., Meyers, D.J., Cole, P.A., and Culig, Z. (2011). Inhibition of the acetyltransferases p300 and CBP reveals a targetable function for p300 in the survival and invasion pathways of prostate cancer cell lines. Molecular Cancer Therapeutics *10*, 1644-1655.

Sebio, A., Kahn, M., and Lenz, H.-J. (2014). The potential of targeting Wnt/β-catenin in colon cancer. Expert Opinion on Therapeutic Targets *18*, 611-615.

Sharma, S.V., Oneyama, C., Yamashita, Y., Nakano, H., Sugawara, K., Hamada, M., Kosaka, N., and Tamaoki, T. (2001). UCS15A, a non-kinase inhibitor of Src signal transduction. Oncogene *20*, 2068-2079.

Sokol, S.Y. (2011). Maintaining embryonic stem cell pluripotency with Wnt signaling (Oxford University Press for The Company of Biologists Limited), pp. 4341-4350.

Song, L., Wang, L., Li, Y., Xiong, H., Wu, J., Li, J., and Li, M. (2010). Sam68 up-regulation correlates with, and its down-regulation inhibits, proliferation and tumourigenicity of breast cancer cells. The Journal of Pathology *222*, 227-237.

Sumithra, B., Saxena, U., and Das, A.B. (2019). A comprehensive study on genome-wide coexpression network of KHDRBS1/Sam68 reveals its cancer and patient-specific association. Scientific reports *9*, 11083-11083.

Takebe, N., Miele, L., Harris, P.J., Jeong, W., Bando, H., Kahn, M., Yang, S.X., and Ivy, S.P. (2015). Targeting Notch, Hedgehog, and Wnt pathways in cancer stem cells: Clinical update, pp. 445-464.

Takemaru, K.I., and Moon, R.T. (2000). The transcriptional coactivator CBP interacts with β-catenin to activate gene expression. Journal of Cell Biology *149*, 249-254.

Tang, Z., Kang, B., Li, C., Chen, T., and Zhang, Z. (2019). GEPIA2: an enhanced web server for large-scale expression profiling and interactive analysis. Nucleic Acids Research *47*, W556-W560.

Taylor, S.J., Anafi, M., Pawson, T., and Shalloway, D. (1995). Functional interaction between c-Src and its mitotic target, Sam 68. Journal of Biological Chemistry *270*, 10120-10124.

Taylor, S.J., and Shalloway, D. (1994). An RNA-binding protein associated with Src through its SH2 and SH3 domains in mitosis. Nature *368*, 867-871.

Todaro, M., Alea, M.P., Di Stefano, A.B., Cammareri, P., Vermeulen, L., Iovino, F., Tripodo, C., Russo, A., Gulotta, G., Medema, J.P*., et al.* (2007). Colon Cancer Stem Cells Dictate Tumor Growth and Resist Cell Death by Production of Interleukin-4. Cell Stem Cell *1*, 389-402.

Trott, O., and Olson, A.J. (2010). AutoDock Vina: improving the speed and accuracy of docking with a new scoring function, efficient optimization and multithreading. J Comput Chem *31*, 455-461.

Tuveson, D., and Clevers, H. (2019). Cancer modeling meets human organoid technology (American Association for the Advancement of Science), pp. 952-955.

Van De Wetering, M., Sancho, E., Verweij, C., De Lau, W., Oving, I., Hurlstone, A., Van Der Horn, K., Batlle, E., Coudreuse, D., Haramis, A.-P*., et al.* (2002). The-Catenin/TCF-4 Complex Imposes a Crypt Progenitor Phenotype on Colorectal Cancer Cells renewal occurs in these crypts through a coordinated series of events involving proliferation, differentiation, and migration toward the intestinal lumen. Pluripoten, pp. 241-250.

Van Der Heijden, M., and Vermeulen, L. (2019). Stem cells in homeostasis and cancer of the gut (BioMed Central Ltd.), pp. 66-66.

Vermeulen, L., De Sousa E Melo, F., Van Der Heijden, M., Cameron, K., De Jong, J.H., Borovski, T., Tuynman, J.B., Todaro, M., Merz, C., Rodermond, H*., et al.* (2010). Wnt activity defines colon cancer stem cells and is regulated by the microenvironment. Nature Cell Biology *12*, 468-476.

Werbowetski-Ogilvie, T.E., Bossé, M., Stewart, M., Schnerch, A., Ramos-Mejia, V., Rouleau, A., Wynder, T., Smith, M.J., Dingwall, S., Carter, T*., et al.* (2009). Characterization of human embryonic stem cells with features of neoplastic progression. Nat Biotechnol *27*, 91-97.

Yang, K., Wang, X., Zhang, H., Wang, Z., Nan, G., Li, Y., Zhang, F., Mohammed, M.K., Haydon, R.C., Luu, H.H*., et al.* (2016). The evolving roles of canonical WNT signaling in stem cells and tumorigenesis: Implications in targeted cancer therapies. Laboratory Investigation *96*, 116-136.

Yang, L., Shi, P., Zhao, G., Xu, J., Peng, W., Zhang, J., Zhang, G., Wang, X., Dong, Z., Chen, F*., et al.* (2020). Targeting cancer stem cell pathways for cancer therapy (Springer Nature), pp. 1-35.

Zhan, T., Rindtorff, N., and Boutros, M. (2017). Wnt signaling in cancer. Oncogene *36*, 1461-1473.

Zhang, Z., Li, J., Zheng, H., Yu, C., Chen, J., Liu, Z., Li, M., Zeng, M., Zhou, F., and Song, L.B. (2009). Expression and cytoplasmic localization of SAM68 is a significant and independent prognostic

marker for renal cell carcinoma. Cancer Epidemiology Biomarkers and Prevention *18*, 2685-2693.

Zhou, H., and Skolnick, J. (2012). Template-based protein structure modeling using TASSER(VMT.). Proteins *80*, 352-361.